Title
Fundamental Investigation of Triton Surfactant-Containing Aqueous Two-Phase Systems

Author
Yip, Allison

Publication Date
2016

Peer reviewed|Thesis/dissertation

UNIVERSITY OF CALIFORNIA

Los Angeles

Fundamental Investigation of Triton Surfactant-Containing Aqueous Two-Phase Systems

A thesis submitted in partial satisfaction

of the requirements for the degree Master of Science

in Bioengineering

by

Allison Tin-Yan Yip

2016

ABSTRACT OF THE THESIS

Fundamental Investigation of Triton Surfactant-Containing Aqueous Two-Phase Systems

by

Allison Tin-Yan Yip

Master of Science in Bioengineering

University of California, Los Angeles, 2016

Professor Daniel T. Kamei, Chair

Cervical cancer is the fourth most common cancer in women, with essentially all cases caused by long-lasting infection with high-risk types of the human papillomavirus (HPV). Unlike other cancers, the risk of developing cervical cancer can be greatly reduced with vaccines that protect against infection from these high-risk HPV types. Furthermore, widespread and routine gynecologic screening, such as the Papanicolaou (Pap) test and HPV testing, have significantly decreased the incidence of cervical cancer and deaths from the disease in industrialized countries.

However, despite being potentially preventable and curable, cervical cancer continues to be a leading cause of cancer-related death for women living in regions with limited health care resources. Nearly 85% of all cervical cancer cases occur in less developed regions of the world, and in 2012, almost nine out of ten (87%) cervical cancer related deaths affected women in resource-poor settings. This global disease burden is largely due to the lack of effective cervical cancer screening programs and access to prophylactic vaccines, creating a clear need for new point-of-care (POC) screening technologies for women in developing countries. As such, women in resource-poor communities could greatly benefit from a simple, low-cost, and equipment-free test that can be self-administered and can provide easily interpretable results in a reasonable amount of time.

One common paper-based diagnostic device that has the potential to satisfy the aforementioned criteria is the lateral-flow immunoassay (LFA), a rapid antibody-based test that is most recognized for its application as the over-the-counter pregnancy test. However, despite success in certain applications, the sensitivity of LFA remains inferior in comparison to that of gold-standard diagnostic laboratory assays, limiting its use in more widespread clinical applications. To address this problem, our group has previously utilized various aqueous two-phase systems (ATPSs) to preconcentrate target biomolecules, after which the phase containing the concentrated biomolecule was extracted and applied to LFA for improved detection. Our group has also discovered that by integrating ATPS with LFA, particular types of paper and 3D paper architectures can significantly accelerate the rate of phase separation of an ATPS, leading to shorter assay times and fewer sample preparation steps, in addition to sensitive results.

The focus of this thesis was to investigate various components required to create a new ATPS integrated LFA screening test that could detect for HPV16. This test serves as a precursor

to a commercialized device that could determine if women are at risk for cervical cancer in health care limited settings. One main focus of this thesis was to identify and optimize two ATPS systems that can lyse cells and subsequently concentrate the desired biomarkers. The lysing ability of the nonionic Triton X-114 micellar system and polyethylene glycol (PEG) – potassium phosphate salt (PEG-salt) system with Triton X-100 were studied, and their abilities to phase separate as they flowed through paper were determined. Paper constructs were then optimized to ensure accelerated phase separation on paper such that the ATPS could concentrate desired biomarkers to the front of fluid flow for downstream detection.

After confirming that both ATPS solutions exhibited the desired cell lysis and phase separation properties, the partitioning of model hydrophilic and hydrophobic particles indicative of the size of HPV were studied. A mathematical model was then developed based on thermodynamic principles, and this model considered contributions from excluded-volume and hydrophobic interactions to predict partition coefficients of a particle in a Triton X-114 micellar ATPS. The model reasonably predicted the measured experimental partition coefficient, and can be further developed in the future to provide even more accurate predictions of partition coefficients.

Lastly, the limit of detection of HPV16 L1 was determined with LFA only. Studies suggest that the Triton X-114 micellar system has the potential to improve the detection of HPV16 upon integration with LFA. Additionally, to our knowledge, this is the first successful demonstration of detection of the HPV16 L1 major capsid protein using LFA. In the future, this paper-based device can be further improved to detect for desired cervical cancer biomarkers to provide cervical cancer risk determination results that are both sensitive and quick.

The thesis of Allison Tin-Yan Yip is approved.

Dean Ho

Benjamin M. Wu

Daniel T. Kamei, Committee Chair

University of California, Los Angeles

2016

Dedicated to my mother, father, sister, and brother.

Table of Contents

Acknowledgments

The work in this thesis and my overall development as a researcher would not have been possible without the help of several individuals. I would like to take this moment to first thank my greatest teacher and mentor, Dr. Daniel T. Kamei. His guidance and support has never ceased, and I am forever grateful for the opportunity to learn important lessons, both inside and outside the classroom, from such a hardworking, intelligent, and caring mentor. Dan has constantly challenged and encouraged me to grow into the best version of myself and I do not believe that I would be the person I am today without his guidance and mentorship. In retrospect, pursuing another year of research has been one of the best experiences I have had; this year was more meaningful than anything I could have imagined. It is not often that you find something you are so passionate about that you can continue working 24/7 on it without ever feeling tired. Thank you, Dan, for welcoming me back into the Kamei Lab as a graduate student. I will miss working in your lab.

Next, I would like to thank all my graduate student colleagues who have stood by my side and helped me through my research endeavors this year. Thank you, Dr. Garrett Mosley for being a good role model for others in the lab, a fun person to talk to, and for helping me with my radioactivity experiments. David Pereira, who also helped with my radioactivity experiments, but more importantly is someone who works hard and is a good friend with a similar sense of humor as I. Sherine Cheung, my newest best friend, for guiding me through grad school and being someone who I can count on and be comfortable around. Dan Bradbury, who has always given me good suggestions for my own research (as well as for others in lab) and for becoming a close friend. And lastly, Alison Thach and Kevin Chen, my fellow MS grad student friends. I am happy and grateful that I was able to become closer with all of you guys over this past year.

Additionally, I would like to thank my two undergraduate students, Justin Paek and Eumene Lee. Both of them are dedicated to the lab and never fail to put a smile on my face. Justin and Eumene have both been a pleasure to work with and some of the data in this thesis would not have been possible without their help. They will also be the ones to continue this project after I leave, and I wish them all the best.

I would also like to thank the rest of the Kamei Lab: Andre, Amy, Sam, April, Chloe, Vincent, Coco, Matt, Nguyen, Elizabeth, Erica, and Emily because every day I am thankful that I can come to lab and be surrounded with a group of such bright, motivated, and wonderful people. It is people like them that make Kamei Lab so great.

Lastly, I would like to thank my family. My parents have always been supportive of my academic endeavors and taught me all the values that I hold today. They are also some of the hardest working and most resilient people I know. Thank you Mom and Dad, for always cheering me on and taking care of me. Also, thank you to my younger brother, Evan, who isn't so little anymore. Evan continues to be my main motivator to pursue a career in medicine. I want to learn to become someone who can not only take care of you, but also other people. And last but not least, thank you to my twin sister Meagan. Meagan, you have always been there for me since the start and words cannot express how much I appreciate what you do for me. You know how to brighten my day and understand me on a whole different level.

Curriculum Vitae

Education

Calabasas High School
Calabasas, California
Class of 2010

University of California, Los Angeles
Bachelor of Science in Bioengineering, June 2014
Cum Laude

Publications

B.S. Lee, **A.T. Yip**, A.V. Thach, A.R. Rodriguez, T.J. Deming, and D.T. Kamei, "The encapsulation and targeted delivery of doxorubicin with transferrin-conjugated block copolypeptide vesicles." *Int J Pharm*. Vol. 496, pp. 903-11, December 2015.

R.Y T. Chiu, E. Jue, **A.T. Yip**, A.R. Berg, S.J. Wang, A.R. Kivnick, P.T. Nguyen, and D.T. Kamei, "Simultaneous concentration and detection of biomarkers on paper." *Lab Chip*. Vol. 14, pp. 3021-28, June 2014. Highlighted article.

D.Y. Pereira, **A.T. Yip**, B.S. Lee, and D.T. Kamei. "Modeling mass transfer from carmustine-loaded polymeric implants for malignant gliomas." *J. Lab. Autom.* Vol. 19 no. 1, pp. 19-34, February 2013. Cover article.

1. Introduction

1.1 Cervical Cancer Overview

Cervical cancer is the fourth most prevalent cancer worldwide in women, with an estimated 528,000 new cases in 2012.[1] The cervix is the lower, narrower portion of the uterus within the female reproductive system that leads from the uterine cavity to the vagina. The two main types of cervical cancers are squamous cell carcinoma, which is more prevalent than the second type of cancer called adenocarcinoma. Squamous cell carcinoma is cancer of the thin, flat cells lining the cervix and adenocarcinoma is cancer of the glandular cervical cells that make mucus and other fluids. Almost all cervical cancer cases are caused by long-lasting infection with high-risk types of the human papillomavirus (HPV), although it is also important to note that a majority of women infected with these types of HPV do not develop cervical cancer.[2]

Unlike other cancers, the risk of developing cervical cancer can be greatly reduced with vaccines that protect against infection from these high-risk HPV types. Moreover, widespread and routine gynecologic screening, such as the Papanicolaou (Pap) test and HPV testing, have significantly decreased the incidence of cervical cancer and deaths from the disease in industrialized countries.[3] These cervical cancer screening procedures have allowed health professionals to detect cervical dysplasia as well as early cervical cancers, which can subsequently be treated very successfully.

However, this is not the case in less developed regions where cervical cancer accounts for almost 12% of all female cancers and continues to be a leading cause of cancer-related death. In 2012 alone, nearly 85% of all cervical cancer cases and almost nine out of ten (87%) cervical cancer deaths in the world occurred in low income countries.[1] This is largely due to the lack of effective cervical cancer screening programs and access to prophylactic HPV vaccines, creating

a clear need for new point-of-care (POC) screening technologies for women in developing countries.

1.2 Development of Cervical Cancer

1.2.1 HPV as a Risk Factor

Long-lasting infection with high-risk HPV types is the most important determinant risk factor for cervical cancer as it causes essentially all (99.7%) cervical cancer cases.[4] Globally, HPV is one of the most common sexually transmitted diseases.[2] HPVs are DNA viruses with over 200 identified types, of which, about 40 types infect the mucosal epithelium through sexual intercourse or skin-to-skin contact of genital areas. These sexually transmitted HPV types are categorized as either low-risk or high-risk HPVs according to their relation with cervical cancer. Low-risk HPVs are not carcinogenic, but can cause skin and genital warts. On the other hand, high-risk HPV types can cause cancer if the body is unable to clear the virus, leading to the development of a precancerous lesion that can potentially transform further into cervical cancer. Of around 15 high-risk types of HPV, HPV types 16 and 18 account for approximately 70% of all cervical cancer cases.[5] HPV type 16 (HPV16) in particular has the highest risk for cervical cancer development of all the high-risk HPV types.[2,5] However, it should also be noted that most infections do not transform into cervical cancer as the virus is cleared or suppressed by the body's immune system within 4-18 months after exposure.[6,7]

1.2.2 HPV Virology

The HPV genome includes a non-coding long control region (LCR) responsible for interacting with host cell factors to regulate viral replication and gene expression. In addition, the

HPV genome is comprised of eight overlapping open reading frames, consisting of six early genes (E1, E2, E4, E5, E6, E7) and two late genes (L1, L2). The early genes regulate viral replication while the late genes encode for the major and minor capsid proteins of the virus. Figure 1.1 shown below illustrates the genome for HPV16.

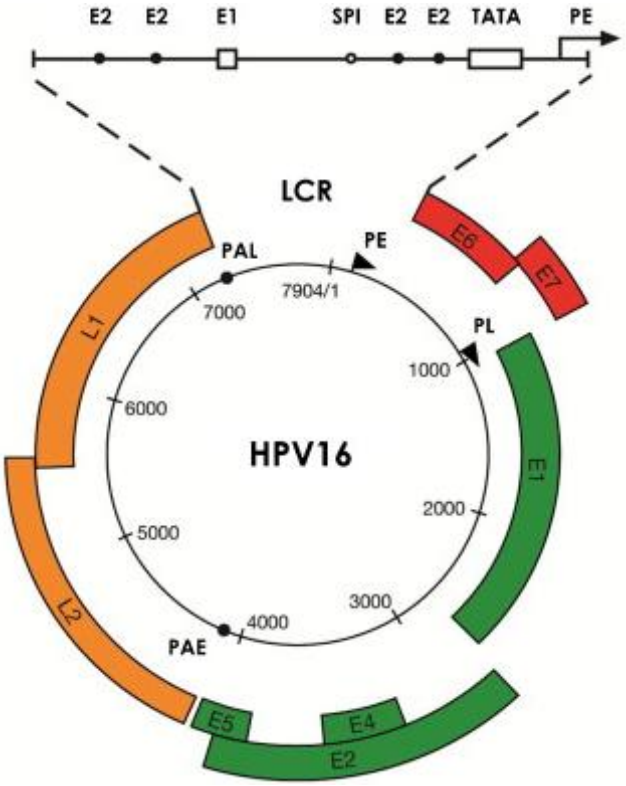

Figure 1.1 The HPV16 genome. The six early genes, E1, E2, E4 and E5, as well as E6 and E7, are shown in green and red, respectively. E6 and E7 are known oncogenic genes. The late genes, L1 and L2, are shown in orange. The long control region (LCR) is enlarged in this image. Reprinted from Vaccine, Volume 30, Doorbar *et al.*, The Biology and Life-Cycle of Human Papillomaviruses, pages F55-F70 (2012) with permission from Elsevier.[8]

Expression patterns of these genes change throughout the HPV life cycle, which begins with infection, followed by sequential stages of genome maintenance, proliferation, genome amplification, viral DNA packaging, and virus release. Abnormal cells typically develop from an

HPV infection in the ring of mucosa called the cervical transformation zone, a junction between the columnar epithelium of the endocervix and the squamous epithelium of the ectocervix. This is an area of constant change where the columnar cells of the basement membrane differentiate and mature into squamous epithelial cells as they migrate toward the upper levels of the epithelium.

1.2.3 Cervical Cancer Pathogenesis

The development of cervical cancer can be divided into four major steps: oncogenic HPV infection in the cervical transformation zone, persistence of the HPV infection, progression of viral infection to precancer in an epithelial cell clone, followed by development of carcinoma and invasion through the basement cell membrane.[9]

Infection first occurs when HPV is introduced through sexual contact and the virus invades the replicating basal cells that are exposed through small tears within the cervical epithelium. In the basal layers, viral HPV DNA establishes and maintains itself as low copy episomal DNA by using host DNA replication machinery or, less commonly, incorporates itself into the host genome. At this stage, viral replication is considered latent and can remain this way for several months or years prior to becoming proliferative.

In the context of cervical cancer, it is well accepted that a persistent and long-lived high-risk HPV infection can cause cancer when it is in a cellular environment conducive to high level expression of viral oncogenes E6 and E7 in the basal or parabasal cells of the epithelium. Overexpression of E6 and E7 is largely responsible for the initiation and progression of cervical cancer because its resulting protein products, also named E6 and E7, disrupt normal cell replication and induces genomic instability through multiple mechanisms. Mainly, E6 and E7

from high-risk HPV have high affinity to tumor suppressor protein p53 and retinoblastoma gene product pRB, respectively. E6 binds to p53 resulting in its rapid degradation by a cellular ubiquitin ligase.[10] This abolishes the normal functions of p53 such as regulation of G_1 arrest in the cell cycle, DNA repair, and apoptosis. Furthermore, E7 inhibition of the retinoblastoma protein (pRB) disturbs cell cycle regulation. Normally, binding of pRB to the E2F family of transcription factors blocks E2F driven cell cycle activation. In cells with transforming HPV infections, E7 interrupts the regulation of the RB-E2F pathway by binding to pRB, thereby rendering it inactive. This leads to the release of E2F from pRB, resulting in continuous activation of the cell cycle. Overall, the functions of E6 and E7 cooperate to bypass normal cell growth regulatory pathways and modify the cellular environment to facilitate viral replication (Figure 1.2).

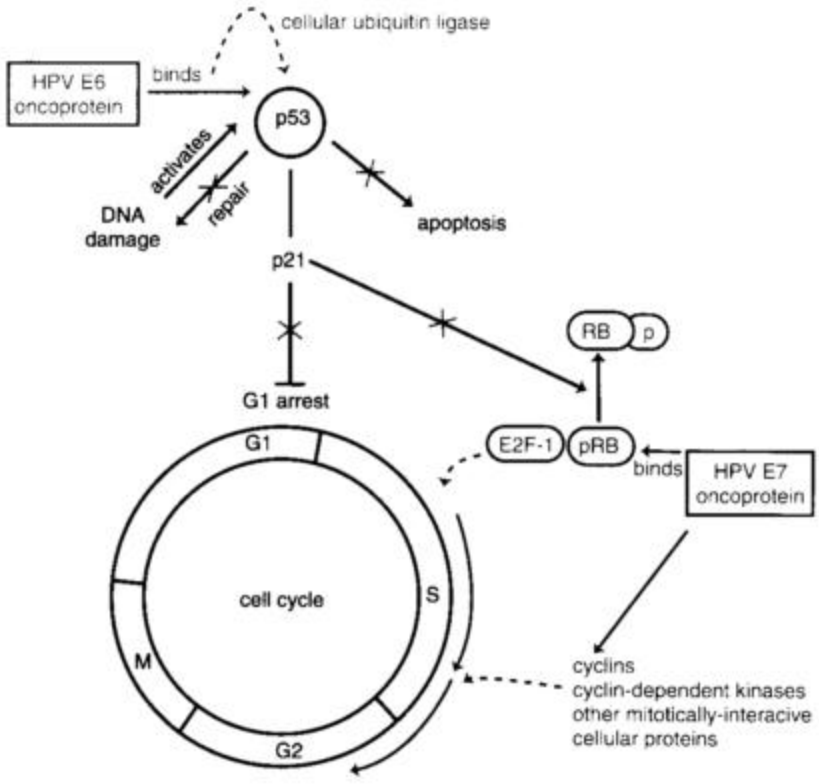

Figure 1.2 The oncogenic pathways of E6 and E7. The protein products of oncogenic genes E6 and E7 act primarily by binding to p53 and pRB, respectively. This results in abnormal cell cycle regulation and ultimately leads to cellular transformation. Adapted from Burd (2003) with permission from American Society for Microbiology. [11]

Differentiation of the basal epithelial cells then triggers the continuation of the viral life cycle, shifting the viral genome expression patterns from early genes to late genes. Genome amplification is followed by the final stages of the viral cycle when the replicated genomes are packaged into infectious particles and released. To reiterate, the late genes encode for the major and minor capsid proteins, L1 and L2, which assemble into the HPV virions in the upper epithelial layers to be released. Release of the infectious virions can go on to further infect other cells.

When considering the bigger picture, the uncontrolled cell replication caused by high-risk HPV leads to the accumulation of abnormal cervical cells that alter the normal cellular architecture of the epithelial tissue. The ordered, structural appearance of the tissue begins to look disorganized and the extent of this disorganization from the bottom basement membrane to the upper layers of the epithelium is used to classify the degree of the cervical intraepithelial neoplasia (CIN). CIN is divided into three grades, CIN1, 2, or 3, and is determined from biopsying of the affected area of the cervix. Abnormal cell growth in the lower one third of the basal epithelium is referred to as CIN1. CIN1 indicates mild changes and in most cases does not lead to cancer. If the abnormalities extend to two thirds of the epithelium, it is CIN2. Lastly if the abnormal cells span greater than two thirds of the epithelium, the lesion is classified as CIN3. CIN3 is the precursor to cervical cancer and becomes invasive once it invades the lower basement membrane. The pathogenesis of cervical cancer is reviewed in Figure 1.3.

Even with CIN2 or CIN3, it is unlikely that the woman has cancer. However, although most HPV infections are cleared by the body and precancerous lesions regress and resolve, there is still a risk for lesions to progress into cervical cancer. Studies have shown that it can take up to 15 to 20 years for cervical cancer to develop from persistent HPV infection.[2]

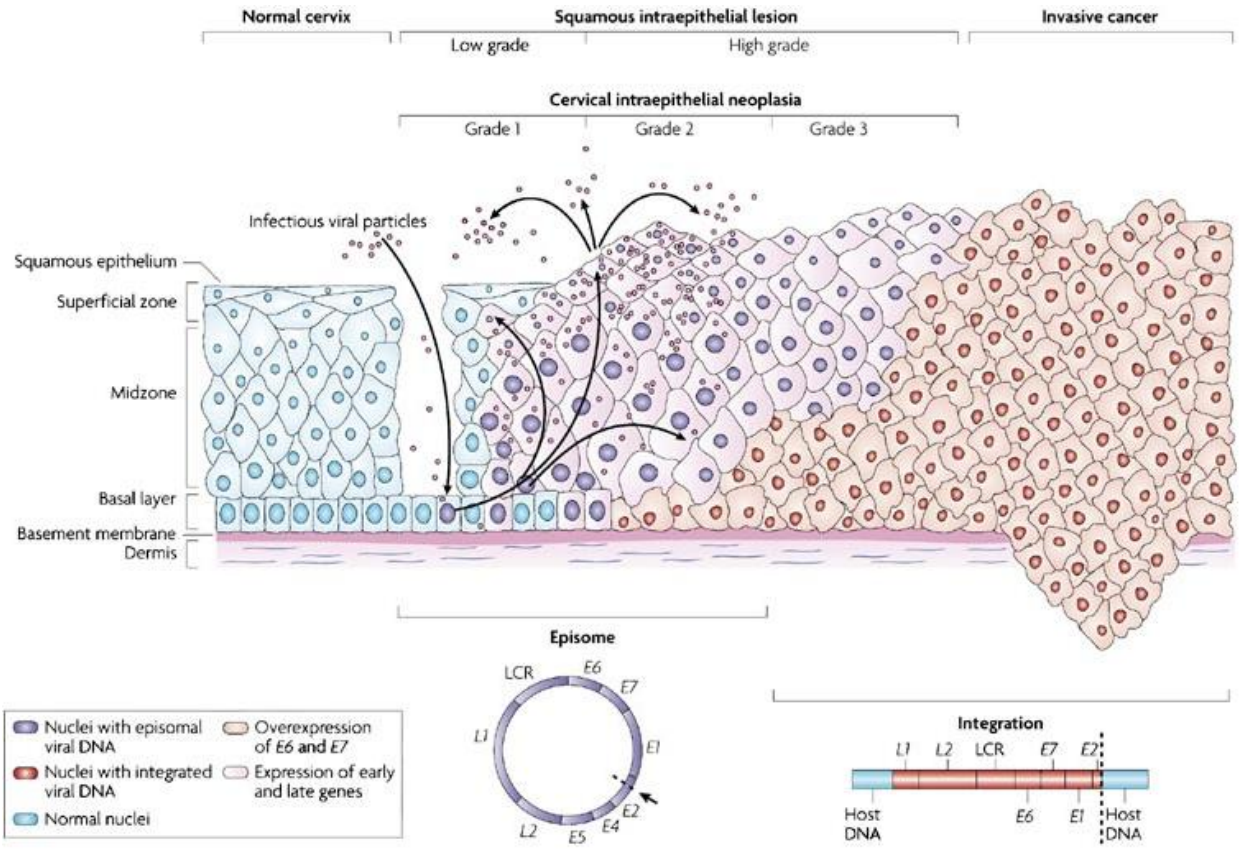

Figure 1.3 Pathogenesis of cervical cancer. Basal cells in the cervical epithelium lie on the basement membrane, which sits above the dermis. HPV gains access to the basal cells through small abrasions in the cervical epithelium and can cause infection. Subsequently, the early HPV genes are expressed and the viral DNA replicates and are maintained as episomal DNA (purple nuclei). In the upper layers of epithelium, the viral genome is replicated further, and the late genes are expressed. L1 and L2 encapsulate the viral genomes to form progeny virions in the nucleus which can be released to initiate a new infection. Low-grade intraepithelial lesions support productive viral replication and can progress to high-grade cervical intraepithelial neoplasia (CIN). The progression of untreated lesions to invasive cancer is associated with upregulation of E6 and E7 oncogene expression. Reprinted by permission from Macmillan Publishers Ltd: *Nature Reviews Cancer*[12], copyright (2007).

1.3 Current Methods of Screening

Cervical screening tests are therefore performed to detect and diagnose cervical dysplasia, helping physicians monitor disease progression and decide if subsequent treatment is needed. When abnormal tissue or cancer is found early, treatment of precancerous lesions

decreases the incidence of cervical cancer and treatment of early-stage cervical cancer decreases mortality.[3] Screening is thus especially important as women often are asymptomatic. In countries with well-established cervical cancer screening programs, the gold-standard method of screening is the Pap/HPV cotest.

1.3.1 Pap Test

The primary method for cervical cancer screening is the Pap test, also known as a Pap smear. This type of cervical cytology screening yields cell-based results and does not provide any information about tissue structure. Diagnosis of CIN, mentioned earlier, would instead require biopsy for histological examination. During the Pap test, a healthcare professional collects cells from the surface of the cervix and vagina using a cotton swab or brush. This is typically performed at a doctor's office during a routine pelvic exam. These cells are then fixed onto a slide and examined under the microscope to identify the presence or absence of abnormal cells in the cervical transformation zone.

There are two acceptable kinds of Pap test procedures, the conventional Pap test and the liquid-based Pap test. Patient specimens collected during the conventional Pap tests are immediately fixed onto a slide, whereas for a liquid-based Pap test, the sampled cells are suspended in a liquid transport medium. Subsequently, the cells are either spun down or filtered prior to being plated as a thin layer on a slide. For the latter Pap test method, HPV testing can be performed on the cells, while that is not possible with the former Pap test. In the United States, it is recommended that women under 30 receive the Pap test every 3 years with initial screening beginning no earlier than age 21. For women 30 years of age or older, a Pap test is recommended

every 3 years or co-testing with the Pap and HPV tests every 5 years if both initial tests are negative.[13]

The current way to report cervical cytology test results uses the Bethesda test naming convention.[14] Test results fall under three general categories: negative for intraepithelial lesion or malignancy, epithelial cell abnormality, or other. Epithelial cell abnormality is further divided into several subcategories (Table 1.1).[14] If considering only squamous cells that are abnormal, they can either be classified as cervical squamous intraepithelial lesion (SIL) or atypical squamous cells (ASC). ASC is considered to be suggestive of SIL but designate cellular abnormalities that quantitatively or qualitatively fall short of the definitive diagnosis of SIL. SIL is divided into low-grade squamous intraepithelial lesion (LSIL) and high-grade squamous intraepithelial lesion (HSIL). LSIL includes patients with HPV infection, mild dysplasia, and CIN1, whereas HSIL encompasses moderate to severe dysplasia, carcinoma in situ, CIN2, and CIN3. For ASC, the cells can be of undetermined significance (ASC-US) or the cells can be classified as ASC where HSIL cannot be excluded (ASC-H). These ASC terms are used to emphasize that some of these cases are associated with underlying CIN2 or CIN3 diagnoses.

Table 1.1: Possible results for epithelial cell abnormalities as defined by the Bethesda system[14]

Epithelial Cell Abnormalities	
Squamous cell	**Glandular cell**
• Atypical squamous cells (ASC) ▪ of undetermined significance (ASC-US) ▪ cannot exclude HSIL (ASC-H) • Low-grade squamous intraepithelial lesion (LSIL) ▪ human papillomavirus (HPV), mild dysplasia, cervical intraepithelial neoplasia (CIN) 1 • High-grade squamous intraepithelial lesion (HSIL) ▪ moderate and severe dysplasia, carcinoma in situ; CIN 2 and CIN 3 • Squamous cell carcinoma	• Atypical glandular cells, favor neoplastic (*endocervical or not otherwise specified*) • Endocervical adenocarcinoma in situ (AIS) • Adenocarcinoma

1.3.2 HPV Testing

HPV testing is used in conjunction with cervical cytology because studies have shown that co-testing has improved sensitivity for detection of cervical cancer precursors like CIN2 and CIN3.[15] HPV tests can distinguish most, but not all, of the high-risk HPV types by either detecting for DNA or mRNA. Currently there are four HPV tests that are approved by the FDA for use in co-testing with a Pap smear: Hybrid Capture 2 (HC2), Cervista HPV HR test, Cobas HPV test, and Aptima mRNA test (Table 1.2). Hybrid capture is a liquid hybridization method and detects for 13 high-risk HPV types. It reports results as positive for one or more of these high-risk types or negative for all. The Cervista HPV HR test uses signal amplification and fluorescence to detect for 14 high-risk HPV types. Test results come back as positive for one or more of the 14 high-risk HPV types by using a 14-probe mix, but Cervista also offers a test to detect specifically for HPV16 and HPV18. The Cobas HPV test utilizes amplification of target DNA by polymerase chain reaction (PCR) and nucleic acid hybridization for the detection of 14

high-risk HPV types. This test can indicate positive for HPV16 and HPV18 individually, with the remaining 12 types detected collectively. Lastly, the HPV test from Aptima is unlike the ones previously described as it detects for mRNA rather than DNA. The Aptima mRNA test targets E6 and E7 mRNA and was recently approved from the FDA as it provides better sensitivity and specificity than HPV DNA testing, particularly for detecting for CIN2 positive.[16]

Table 1.2: FDA approved HPV tests

Test	HPV types detected	Results
Hybrid Capture 2	16, 18, 31, 33, 35, 39, 45, 51, 52, 56, 58, 68	Positive for one or more HPV types
Cervista HPV HR test	16, 18, 31, 33, 35, 39, 45, 51, 52, 56, 58, 66, 68	Positive for one or more HPV types
Cobas HPV test	16, 18, 31, 33, 35, 39, 45, 51, 52, 56, 58, 66, 68	Specific for 16 and 18, with pooled results for the remaining types
Aptima mRNA test	16, 18, 31, 33, 35, 39, 45, 51, 52, 56, 58, 66, 68	Positive for one or more HPV types

1.3.3 Interpretation of Test Results

The aforementioned tests only screen for cellular abnormalities associated with increased risk for cervical cancer development and help health care professionals determine whether or not a patient requires further evaluation. The only exception is the differential diagnosis provided by an HSIL result from cervical cytology. Women requiring further evaluation are typically referred to colposcopy, a procedure in which a lighted magnifying instrument is used to check the vagina and cervix for abnormal areas, and cervical biopsy may be performed. Treatment decisions are then made after receiving diagnostic results from histological examination of cervical specimens taken from biopsy.

With this medical algorithm, patient prognoses in developed countries tend to be good because cervical cancer screening of women is well established and rigorous. However, this gold-standard method of screening is impractical or unavailable for women in resource-limited countries.

1.4 Need for Alternative Diagnostics in Resource-Poor Settings

In the developing world, cervical cancer is the second most common cancer with an estimated 445,000 new cases in 2012, accounting for around 85% of new cancer cases worldwide.[1,2] This disproportionate share of disease burden for cervical cancer in the developing world is largely due to the lack of effective screening programs and options aimed at detecting and treating precancerous HPV lesions. Once the HPV infection has progressed to an invasive stage, the disease often proves fatal, especially for patients without access to appropriate surgical, radiotherapy, or chemotherapy treatments. As a result, cervical cancer remains responsible for one of the highest number of cancer-related deaths in resource-limited countries.[1] There is a clear need for an alternative approach in resource-poor regions where it is unfeasible to implement conventional cervical cancer screening methods due to limited access to electricity, laboratory equipment, trained personnel, and convenient healthcare infrastructure. As most HPV infected women are asymptomatic, new diagnostic testing must be both sufficiently specific and sensitive. This is critical for early risk detection to guide an individual to seek further assessment and subsequent treatment. Moreover, new tests can improve the specificity and positive predictive value not provided by current HPV testing as well as circumvent the considerable inter-observer variability in interpretation of Pap smear results. Women in the developing world

instead require an equipment-free diagnostic device that is rapid, user-friendly, low-cost, easy-to-interpret, and applicable at the POC.

One common paper-based diagnostic device that satisfies the aforementioned criteria is the lateral-flow immunoassay (LFA). This rapid, antibody-based test provides clear results about the presence or absence of a biomarker within a sample. A paper-based analytical device can address the unique challenges present in resource-poor settings since paper is readily available, affordable, and provides an intrinsic wicking mechanism that can quickly transport fluids without the aid of an additional pumping device.

There have already been efforts to create an LFA for the purpose of cervical cancer screening. The Arbor Vita Corporation has developed the OncoE6 Cervical Test that detects for the E6 oncoprotein which requires only limited infrastructure and yields results in just over two hours. In one study performed with a large population of women ages 25 to 65 years living in rural China, the OncoE6 test had a higher positive predictive value of 40.8% for $CIN3^{+}$ when compared to conventional HPV testing, but only a sensitivity of 53.5%.[17] In the follow-up data analysis published from the same study, the authors state that these result highlight that fact that the OncoE6 Cervical Test may be better as a diagnostic test for detection of precancer and cancer in HPV positive women, rather than for screening.[18] This demonstrates the continued difficulty in creating LFA tests with sensitivities necessary for accurately detecting biomarkers of clinical relevance. Despite numerous successful applications, including over-the-counter pregnancy tests and urine drug test kits, the detection limit of LFA is still inferior in comparison to that of gold-standard diagnostic laboratory assays.

However, our lab has previously shown that the limit of detection of LFA can be improved by concentrating target proteins and viruses in a sample with an aqueous two-phase

system (ATPS) prior to detection.[19–22] Moreover, our lab has been developing paper-based diagnostic platforms by integrating an ATPS into LFA such that the device is also able to concentrate biomarkers as a sample is wicked through the paper, demonstrating a 10-fold improvement in the detection limit of a model protein using both a polymer-salt and micellar ATPS.[23,24]

Here, we extend this new ATPS/LFA diagnostic platform for cervical cancer screening by detecting for HPV16. The later iterations of this device would have the potential to be a product that is appropriate for use at the POC and would not only allow women to screen themselves for cervical cancer risk in the comfort of their own homes, but also improve patient outcomes by providing a tool to easily increase the frequency of preventative screenings.

2. Fundamental Investigation of Aqueous Two-Phase Systems: Lysis, Partitioning, and Flow on Paper

2.1 Motivation and Background

Despite being potentially preventable and curable, cervical cancer continues to be a leading cause of cancer-related death for women living in regions with limited health care resources. This is mainly due to the lack of effective cervical cancer screening programs in developing countries, motivating the need for new cervical cancer screening approaches that can address the challenges in resource-poor settings. Cervical cancer screening has traditionally involved direct sampling of the cervix by a health care provider, which poses numerous physical and financial barriers in low income countries. Additionally, most low income countries do not have adequate access to the prophylactic HPV vaccines that can significantly reduce the risk for cervical cancer development. Accordingly, women in resource-poor communities could greatly benefit from a simple, low-cost, and equipment-free test that can be self-administered and can provide easily interpretable results in a reasonable amount of time.

The focus of this thesis was to investigate various components required to create a new ATPS integrated LFA screening test that could detect for HPV16. This test serves as a precursor to a commercialized device that could rapidly determine if women are at risk for cervical cancer in the future. The main focus of this chapter was to identify and optimize two ATPS systems that can lyse cells and subsequently concentrate the desired biomarkers. The lysing ability of the nonionic Triton X-114 micellar system and polyethylene glycol (PEG) – potassium phosphate salt (PEG-salt) system with Triton X-100 were studied, and their abilities to phase separate as they flowed through paper were determined. Paper constructs were then optimized to ensure accelerated phase separation on paper such that the ATPS could concentrate desired biomarkers

to the front of fluid flow for downstream detection. Partitioning studies were also performed using both hydrophobic and hydrophilic particles indicative of the size of HPV.

2.1.1 Aqueous Two-Phase Systems (ATPSs)

In order to enhance the detection limit of LFA to achieve higher sensitivity, target biomolecules can be concentrated using an aqueous two-phase system (ATPS) before detection with LFA. An ATPS is a liquid-liquid extraction system that is compatible with POC diagnostic devices as it is affordable, potentially equipment-free, and provides a mild environment for biomolecules since both phases are comprised mostly of water, unlike conventional oil-water solvent extraction methods.

Biomolecules have been found to partition, or distribute, between the two phases of an ATPS based on their physico-chemical properties such as hydrophobicity and size. Manipulation of the volume ratio, defined as the ratio of the volume of the top phase to the volume of the bottom phase, can result in higher concentration of the desired biomarker. For example, if a biomolecule partitions entirely into the bottom phase of an ATPS, a 9:1 volume ratio ATPS would yield a 10-fold concentration after phase separation as the bottom phase is now $1/10^{th}$ the size of the original total volume. This thesis investigates the use of a polymer-salt-surfactant ATPS and a micellar ATPS for concentration of HPV16 L1.

2.1.2 Polymer-Salt Aqueous Two-Phase System

Certain mixtures of specific polymer and salts have been found to form ATPSs. Here, we utilize the polyethylene glycol (PEG) – potassium phosphate salt, hereon referred to as the PEG-salt ATPS. At specific concentrations of PEG and potassium phosphate, the PEG-salt ATPS

phase separates into a top, more hydrophobic, PEG-rich phase and a bottom, more hydrophilic, salt-rich phase. It should be noted that both the top and bottom phases will contain both the polymer and salt, although the concentration of each species will differ between the top PEG-rich phase and bottom salt-rich phase. More specifically, the top phase is PEG-rich and salt-poor, whereas the bottom phase is PEG-poor and salt-rich. Determining the final concentration of PEG and salt in each phase is possible by looking at a phase diagram, which is set at a constant temperature (Figure 2.1.1). For these phase diagrams, the y and x-axes represents the concentration of polymer and potassium phosphate salt, respectively. At operating conditions above the binodal curve, solutions will phase separate whereas initial operating conditions below the curve are conditions in which the solution will remain a single phase. The concentrations of the phase forming components can then be determined by drawing a tie-line that contains the initial operating condition while intersecting the boundaries of the binodal curve at two points; those two points will determine the concentrations of the polymer and salt in each phase after the ATPS has reached equilibrium. Accordingly, all operating conditions that sit on the same tie-line will result in the same concentrations of both the polymer and salt in both the top and bottom phases. These initial concentrations, however, alter the resulting volume ratio of the ATPS solution. The tie-line provides information about the volume ratio simply by using the lever rule. The lever rule is an extension of a mass balance calculation, and thus the proportion of the final macroscopic phases is given by the relative lengths of the tie line. For example, when considering a PEG-salt ATPS, the line segment on the right side of the tie-line gives the proportion of the top, PEG-rich phase, while the line segment of the left side of the tie-line gives the proportion of the bottom, salt-rich phase.

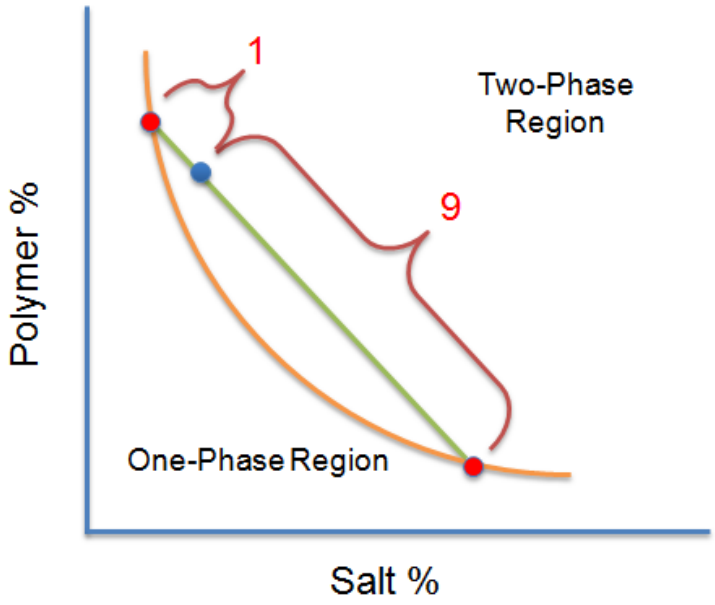

Figure 2.1.1 Schematic of a generalized binodal phase diagram for a general polymer-salt ATPS. Here, the initial operating condition (denoted by the point in blue) phase separates into a 9:1 volume ratio ATPS as determined by the lever rule after drawing the green tie line.

The formation of the two immiscible phases in the PEG-salt ATPS can be viewed microscopically and macroscopically. On a molecular level, PEG polymers in an aqueous solution are surrounded by a hydration shell due to the ether oxygen present in its repeating ethylene glycol unit, permitting hydrogen bonding with surrounding water molecules. When salt is present at a high enough concentration in the same aqueous environment, the salt ions disrupt the hydration shell and dehydrates the ethylene oxide units by drawing water molecules away from the PEG. This allows the PEG polymers to experience more favorable van der Waals interactions with other PEG polymers since the PEG-water interactions are now less favorable in the presence of salt. Macroscopically, this allows the formation of PEG-rich domains that can coexist with PEG-poor (salt-rich) domains which eventually coalesce together to minimize interfacial surface area due to the interfacial tension. As a result, domains move up or down

according to density differences between the domains to ultimately form two macroscopically distinct phases at equilibrium.

For the PEG-salt ATPS, the HPV virion is expected to partition extremely into the bottom salt-rich phase (Figure 2.1.2). The virus is hydrophilic and should preferentially partition into the more hydrophilic salt-rich phase. Additionally, due to its size of about 50-60 nm[25], viral particles will also avoid the top PEG-rich phase as it experiences greater unfavorable excluded-volume interactions with the more abundant PEG molecules in the top, PEG-rich, salt-poor phase. The bottom salt-rich phase containing the concentrated virus of interest can then be applied to LFA to improve the sensitivity of test results.

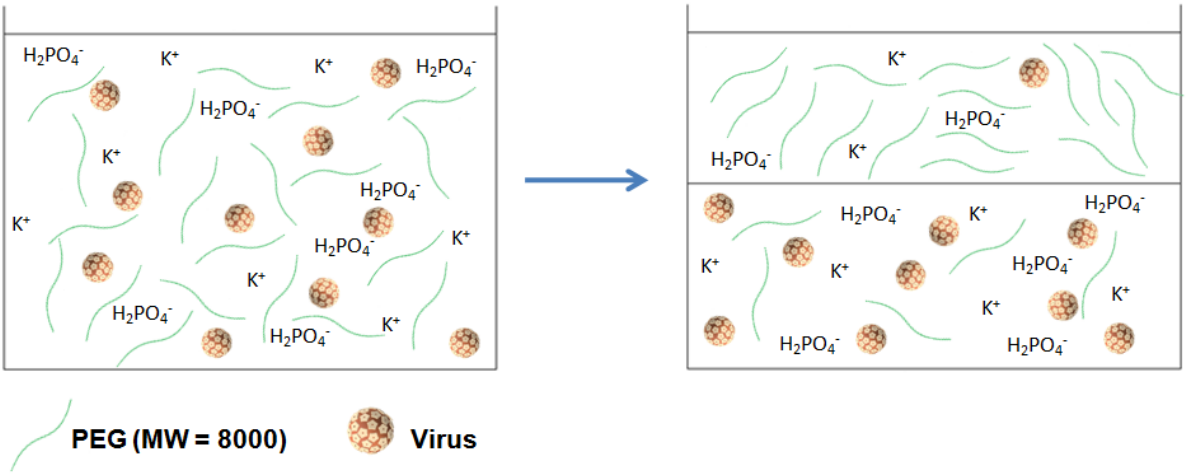

Figure 2.1.2 Partitioning of a virus in PEG-potassium phosphate salt (PEG-salt) ATPS. The PEG-salt ATPS phase separates into a top, PEG-rich phase and a bottom, salt-rich phase (shown on the right). After phase separation, the HPV virions are expected to partition extremely into the bottom, salt-rich phase.

2.1.3 Micellar Aqueous Two-Phase System

Another type of ATPS is a micellar ATPS, which is composed mainly of water and surfactant. Surfactants are amphiphilic molecules that self-assemble into micelles in aqueous

solutions when the concentration of surfactant is above the critical micelle concentration (CMC). Surfactant molecules in micelles are oriented such that the hydrophobic tails point inward to form the core of the micelle while the hydrophilic heads are exposed to water. When the temperature of an aqueous surfactant solution is raised above the critical temperature (T_c), which is specific for each surfactant, the system phase separates into micelle-rich and micelle-poor phases. Likewise, a coexistence curve (Figure 2.1.3) can be used to characterize the ATPS and the volume ratio can be determined using the lever rule. The non-intuitive part of the lever rule is that the length of the line segment used to determine the relative volume ratios is furthest from the phase in which you are interested.

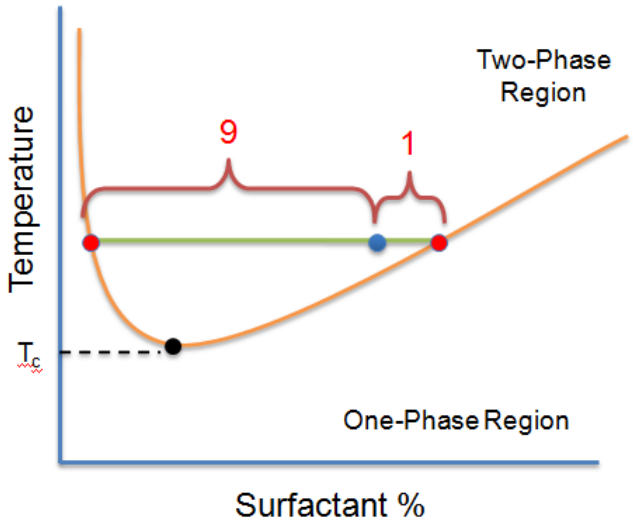

Figure 2.1.3 Generalized coexistence curve for a micellar ATPS. All conditions that exist above the coexistence curve (in orange) will phase separate into two distinct macroscopic phases. The critical temperature T_c (denoted by the black point) is specific for every surfactant and denotes the minimum temperature when phase separation occurs for this ATPS. In this example, the initial operating condition (denoted by the point in blue) phase separates into a 1:9 volume ratio micellar ATPS.

In particular, this thesis focuses on the use of the nonionic Triton X-114 micellar system. Aqueous solutions of Triton X-114 exist as a single, isotropic phase at low temperatures but phase separates into a top micelle-poor phase and a bottom micelle-rich phase upon increasing the temperature past its cloud point. The cloud point is the temperature at which any operating condition becomes turbid, suggesting that the formation of micelle-poor and micelle-rich domains have begun forming. The increase in temperature correspondingly increases the thermal energy of the molecules, disrupting the directionality of hydrogen bonds formed between the water molecules and hydrophilic heads of the micelles. Under these circumstances, the micelles can then experience more attractive van der Waals interactions with other micelles since micelle-water interactions have become less favorable. Similarly to the polymer-salt ATPS discussed earlier, this results in the formation of micelle-poor and micelle-rich domains which coalesce into two macroscopically distinct phases.

As opposed to the PEG-salt ATPS, the HPV virion is expected to partition extremely into the top phase, since in this case, the top phase is micelle-poor for the Trition X-114 micellar ATPS (Figure 2.1.4). Due to its hydrophilicity and size, the virus will prefer to be in the more hydrophilic micelle-poor phase, where it will experience fewer excluded-volume interactions with the fewer micelles in the top, micelle-poor phase.

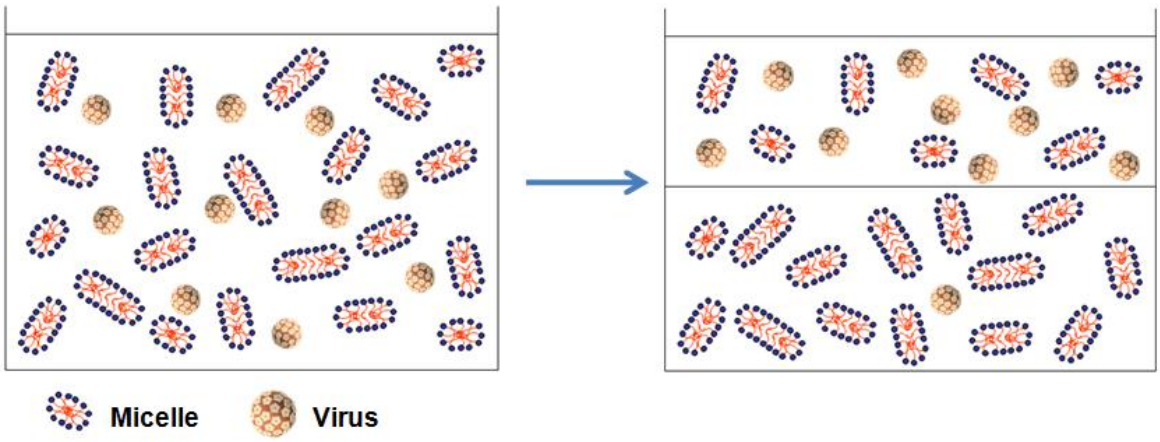

Figure 2.1.4 Partitioning of a virus in the Triton X-114 micellar ATPS. This ATPS phase separates into a top, micelle-poor phase and a bottom, micelle-rich phase (shown on the right). After phase separation, the HPV virions are expected to partition extremely into the top, micelle-poor phase.

2.2. Materials and Methods

2.2.1 Preparation of PEG-Salt ATPS Solutions with Triton X-100

PEG-salt ATPS solutions were prepared with 0.1% of nonionic Trition X-100 (MP Biomedicals, Santa Ana, CA) for all experiments. A low concentration of surfactant was required to confer cell lysing ability to the PEG-salt ATPS, which typically cannot lyse cells. First, polyethylene glycol 8000 (PEG) (VWR, Brisbane, CA) and potassium phosphate salt (5:1 dibasic to monobasic ratio) (Sigma-Aldrich, St. Louis, MO), were dissolved in Dulbecco's PBS (pH 7.4, containing 1.47 mM KH2PO4, 8.1 mM Na2HPO4, 137.92mMNaCl, 2.67 mMKCl, and 0.49 mM MgCl2) (Invitrogen, Grand Island, NY). Solutions were left out at room temperature until they reached equilibrium, as indicated by phases without turbidity and with constant volumes. The volumes of the top phase and bottom phase were measured by marking the outside of the tube at the interface and at the top of the solution. These tubes were then emptied, dried, and weighed on a scale. Water was added up to the markings, and the volumes of both phases were determined using 1 g/mL as the density of water. The 1:1 and 9:1volume ratios were found

by varying the w/w compositions of PEG and salt. The operating conditions were determined to be 12.5% (w/w) PEG, 7.5% (w/w) salt, and 0.1% Triton X-100 for the 1:1 volume ratio solution and 16.76% (w/w) PEG, 4.92% (w/w) salt, and 0.1% Triton X-100 for the 9:1 volume ratio solution.

2.2.2 Preparation of Triton X-114 Micellar ATPS Solutions

The Triton X-114 micellar ATPS were prepared by adding Triton X-114 (Sigma Aldrich, St. Louis, MO) to PBS. The solution was made to be homogeneous through three repetitions of vortexing and icing prior to incubating the solution in a 25°C water bath. Volume ratios were ascertained after the solutions reached equilibrium in a method similar to how the PEG-salt volume ratios were measured. The operating conditions to yield 1:1 and 1:9 volume ratio solutions were found to be 4% (w/w) Triton X-114 in PBS and 7.4% (w/w) Triton X-114 in PBS, respectively.

2.2.3 Determination of Lysing Abilities of ATPS Solutions

The cell lysing abilities of the PEG-salt ATPS with Triton X-100 and the Triton X-114 micellar ATPS were determined by quantifying the amount of protein extracted from HeLa cells (ATCC, Manassas, VA). Once confluent, HeLa cells were counted and 1 x 10^6 cells were placed in a microcentrifuge tube and pelleted via centrifugation at 2,000 x g for 5 min. Cells were washed with PBS to remove substances that could potentially interfere with the subsequent protein quantification assay and pelleted once more by centrifuging at 2,000 x g for 5 min. Subsequently, 1 mL of the appropriate lysing reagent was added to the cells for 5 minutes. The lysing reagents that were tested were as follows: 1:1 and 9:1 PEG-salt with Triton X-100, 1:1

and 1:9 Triton X-114 ATPS, and PBS and 1% (w/w) Triton X-100 as the negative and positive controls, respectively. All the ATPS solutions were homogenous when added to the HeLa cells. Microcentrifuge tubes with the cells and lysing reagents then sat at room temperature for the 5 min incubation time, with the exception of the cells with the Triton X-114 ATPS, which was incubated in a 25°C water bath. The cell lysates for all conditions were clarified by centrifugation at 14,000 x g for 10 min at 4°C and the supernatant was collected for protein quantification. For the PEG-salt ATPSs, the top and bottom phases were collected separately, but the total protein extracted is reported as protein quantified from both phases. For the Triton X-114 ATPSs, the supernatant remained homogenous since the cell lysate is spun at 4°C, a temperature below the cloud point.

Next, protein concentration was determined by using the Pierce BCA Protein Assay (Thermo Fisher Scientific, Waltham, MA) with a bovine serum albumin (BSA) standard curve. This detergent-compatible assay method combines the biuret reaction, the reduction of Cu^{+2} to Cu^{+1} by protein in an alkaline medium, with the highly selective and sensitive colorimetric detection of Cu^{+1} using the bicinchonic acid (BCA) containing reagent.[26] The reaction produces a purple-colored product formed by the chelation of two molecules of BCA with one Cu^{+1}, however this color continues to develop overtime. The rate of continued color development is sufficiently slow unless incubated at higher temperatures. The resulting protein mass was calculated by multiplying the protein concentration by the volume.

Briefly, 25 μL of the sample were placed in a 96 well plate and 200 μL of the BCA assay working reagent were added. The 96 well plate including both the unknown sample solution and BSA standards were incubated at 37°C for 30 min and then cooled to room temperature before reading the absorbance at 560 nm. The protocol was slightly modified for determining the

concentration of the supernatant from the Triton X-114 ATPSs. Since the BCA assay can only tolerate a maximum of 1% Triton X-114 in the sample solution, the supernatant was diluted 10-fold in water and the actual protein concentration was determined by multiplying the calculated value by a factor of 10. Another concern was that incubating the 96 well plate at 37°C could trigger phase separation, therefore two alternative methods were used. In the first approach, the 10-fold diluted, Triton X-114 ATPS supernatant samples were incubated at room temperature with the working reagent for 2 hours and placed on ice briefly to get rid of any turbidity prior to reading absorbance. The second approach involved allowing these samples to sit with the working reagent overnight at 4°C, which ensured that the sample wells did not become turbid but allowed enough time for the reaction to occur, before reading the absorbance at 560 nm.

2.2.4 Preparation of BSA-Coated Gold Nanoparticles (BSA-GNs)

BSA-coated gold nanoparticles (BSA-GNs), which appear dark red due to surface plasmon resonance[27], were used to visualize either the bottom phase of the PEG-salt ATPS with Triton X-100 or the top phase of the Triton X-114 micellar ATPS. The BSA-GNs were made as follows. First, gold nanoparticles were synthesized according to Frens with minor modifications.[28] Briefly, 10 mL of filtered UltraPure sterile water (Rockland Immunochemicals Inc., Gilbertsville, PA) were heated to a boil and then stirred. After which, 100 μL of 1% (w/v) gold (III) chloride hydrate (Sigma Aldrich, St. Louis, MO) were added. After 1 min, 90 μL of 6% (w/v) of sodium citrate monobasic (Sigma Aldrich, St. Louis, MO) were added and allowed to stand and stir on the hot plate for another 2 min. The resulting gold nanoparticles appeared as a dark cherry-red colored suspension. BSA was conjugated onto the gold nanoparticles to form BSA-GNs by taking 1 mL of the gold nanoparticles and adjusting the pH to approximately 7.0-

8.0 by adding 60 μL of 0.1 M sodium borate buffer (pH 9.0). After adjusting the pH, 200 μL of 10% (w/v) BSA in water were added and the mixture was placed on a shaker for 30 min and then pelleted by spinning at 11,000 rpm for 30 min. Free BSA was removed by discarding the supernatant and resuspending the pellet in 200 μL of 1% (w/v) BSA in water. The centrifugation and resuspension step was then repeated twice more. Three pellets were combined and resuspended in 100 μL of 0.1 M sodium borate buffer at pH 9.0 to yield a suspension that was 30 times more concentrated than the original gold nanoparticle solution.

2.2.5 Visualization of ATPS Phase Separation in Test Tube and on Paper

In order to visualize the two phases of the ATPS, BSA-GNs and Brilliant Blue FCF dye (Kroger Co., Cincinnati, OH) were added to the 9:1 volume ratio PEG-salt ATPS with Triton X-100 as well as the 1:9 volume ratio Triton X-114 micellar ATPS. Both types of ATPSs were made to a total solution of 3 g. The 9:1 volume ratio PEG-salt ATPS with Triton X-100 was well-mixed through vortexing and incubated at room temperature while the 1:9 volume ratio Triton X-114 ATPS was well-mixed through vortexing and icing prior to incubation in a 25°C water bath. Images were captured as the solutions phase separated.

Subsequently, the accelerated phase separation that occurs when the ATPS solutions are placed on paper was additionally studied. A 3D paper wick assembled from fiberglass paper (Whatman Intl, Maidstone, England) was prepared by layering four strips of 2 x 0.5 cm fiberglass paper on top of one edge of a 7 x 0.5 cm strip of fiberglass paper that was placed on an adhesive vinyl backing. In particular for the PEG-salt ATPS with Triton X-100, the four strips of 2 x 0.5 cm fiberglass of the 3D paper wick were treated with 0.1% (w/v) sodium cholate in PBS and put under low pressure vacuum overnight. The 3D paper wick was held together by tightly

wrapping a piece of tape around all the strips of paper. Both the 9:1 volume ratio PEG-salt ATPS with Triton X-100 as well as the 1:9 volume ratio Triton X-114 micellar ATPS with BSA-GNs and Brilliant Blue FCF dye were made to 250 mg. The 3D paper wick was placed into the ATPS solutions and images were captured as the solutions simultaneously flowed and phase separated in the paper.

2.2.6 Radiolabeling of Anti-Transferrin Antibody and Tf

A series of partitioning experiments with both hydrophobic and hydrophilic particles were performed with the ATPS solutions. Specifically, to determine the partition coefficient of a hydrophilic particle within the Triton X-114 micellar ATPS, radioactivity was used to measure the amount of dextran-coated gold nanoprobes (DGNPs) that have been functionalized with radiolabeled anti-human transferrin (Tf) antibodies in the top and bottom phases of the 1:1 volume ratio Triton X-114 micellar ATPS.

Briefly, radioactive $Na^{125}I$ (MP Biomedicals, Irvine, CA) was activated by IODO-BEADS (Pierce Biotechnology, Rockford, IL) and then reacted with 100 μg of the polyclonal anti-Tf antibody (Bethyl Laboratories, Montgomery, TX) for 15 min to allow conjugation to the tyrosine residues of the antibody. The radiolabeled anti-Tf antibodies were then purified from free iodine-125 using a Sephadex G10 (Sigma Aldrich, St. Louis, MO) size-exclusion column in the presence of BSA to inhibit nonspecific binding to the column. The phosphotungstic acid (PTA) assay was used to quantify the specific activity and concentration of the radiolabeled antibody.

2.2.7 Preparation of Radiolabeled Gold Nanoprobes

For the purposes of measuring the partition coefficient of a model hydrophilic particle, dextran-coated gold nanoparticles were conjugated with radiolabeled anti-Tf antibodies. First, dextran-coated gold nanoparticles were synthesized according to Min and coworkers with slight modifications.[29] Briefly, 6 g of dextran (MW 15,000-25,000) from Leuconostoc spp. (Sigma Aldrich, St. Louis, MO) were dissolved in 80 mL of filtered UltraPure sterile water (Rockland Immunochemicals Inc., Gilbertsville, PA). The solution was stirred and heated to a boil, after which 1080 μL of a 1% w/v gold (III) chloride hydrate solution were added. The color of the reaction mixture turned reddish-violet and was stirred and boiled for another 20 min. The newly formed dextran-coated gold nanoparticles were centrifuged to remove free dextran and resuspended in 70 mL of water. To form radiolabeled DGNPs, the pH of the dextran-coated gold nanoparticle solution was adjusted to 9.0 using 1.5 M NaOH. For every 1 mL of dextran-coated gold nanoparticle solution, 8 μg of the radiolabeled anti-Tf antibodies were added. The reaction mixture was placed on a shaker for 30 min to facilitate the formation of dative bonds between the antibodies and the dextran-coated gold nanoparticles. Free antibodies were removed by centrifugation. The pellet was resuspended in 100 μL of 0.1 M sodium borate buffer at pH 9.0, and these antibody-decorated dextran-coated gold nanoprobes will be referred to as DGNPs.

2.2.8 Determining Partition Coefficients

The partitioning of two model particles, one hydrophobic and one hydrophilic, was studied in the ATPS solutions. First, the partitioning of 50 nm green fluorescent, carboxylic acid functionalized polystyrene beads (Phosphorex, Hopkinton, MA) were studied in the 1:1 volume ratio PEG-salt ATPS with Triton X-100 and the 1:1 volume ratio Triton X-114 micellar ATPS. Concentrations of these hydrophobic polystyrene beads were determined by measuring the

fluorescence and comparing the values to a standard curve. Standard curves were made to account for the interference of the other components of the ATPS solutions. Specifically, 100 μL of the polystyrene nanoparticles were added to top off 1 g of both the 1:1 volume ratio ATPSs. The solutions were incubated overnight in a 25°C water bath, and the top and bottom phases were separately extracted. Thereafter, each phase was diluted 2-fold and 100 μL of each phase was placed in a 96 well plate for fluorescence measurement with a Tecan Infinite F200 plate reader (Tecan, Männedorf, Switzerland). For the polystyrene beads, fluorescence was measured with an excitation wavelength at 485 nm and an emission wavelength at 535 nm at a gain of 44.

The partitioning of the hydrophilic DGNPs was measured using radioactivity. 5 μL of DGNPs bound to radiolabeled anti-Tf antibodies were added to complete 1 g of a 1:1 volume ratio Triton X-114 micellar ATPS. To ensure that each solution was homogeneous, all suspensions were equilibrated to 4°C prior to incubation in a 25°C water bath. Both phases were carefully withdrawn and the radioactivity (cpm) in each phase was measured using the Packard Cobra Series Auto-Gamma Counter (PerkinElmer, Waltham, MA).

2.3. Results and Discussion

2.3.1 Verifying the Lysing Abilities of ATPSs

To assess cervical cancer risk in women, we envision that our final paper-based ATPS incorporated LFA device will not only be able to detect for high risk HPV16 itself, but also co-test for two other protein biomarkers, p16 INK4a (p16) and Ki-67. Since HPV remains a common sexually transmitted infection, additional detection of these two biomarkers has the potential to increase the specificity of diagnosing precancerous lesions. The p16 molecule is a cyclin dependent kinase inhibitor which is overexpressed as a consequence of deregulated cell

replication due to E7 oncoprotein activity.[16] Ki-67 is a nuclear protein associated with cell proliferation and the fraction of Ki-67 positive tumor cells is often correlated to progression of disease.[30] Researchers have shown that co-staining for p16 and Ki-67 in histological cervical samples has the ability to distinguish a transforming HPV infection from a transient or regressing HPV infection.[31–33]

For this reason, we are interested in utilizing and investigating ATPSs that can lyse cells as both p16 and Ki-67 are intracellular target biomarkers, and HPV may also reside inside cervical cells just prior to viral release. The two types of ATPSs investigated were the PEG-potassium phosphate salt (PEG-salt) ATPS with Triton X-100 as well as the Triton X-114 micellar ATPS. The lysing ability of each ATPS was verified by incubating cervical cancer HeLa cells with the ATPSs and measuring the release of protein.

One of the two ATPS systems studied included the 1:1 and 9:1 volume ratio PEG-salt ATPS with Triton X-100. Typically, a PEG-salt ATPS does not contain any components that can initiate cell lysis. Therefore, a small amount of the nonionic Triton X-100 was spiked into the PEG-salt ATPS to add a lysing capability to an ATPS that is already advantageous in many respects, as it is rather robust because its phase separation behavior is not too sensitive to temperature or minor concentration changes to phase forming components. Most lysis reagent recipes contain Triton X-100, with a concentration ranging from as low as 0.1% to 1% Triton X-100. The lower concentration of 0.1% Triton X-100 is typically sufficient to lyse cells without significantly inhibiting activity of extracted enzymes, although enzymatic activity may still remain for concentrations up to 1% Triton X-100. To be conservative, 0.1% Triton was selected as it served its intended purpose to lyse cells without significantly altering the resulting volume ratio or negatively affecting phase separation behavior of the PEG-salt ATPS. Qualitative tests

done separately suggested that the addition of Triton X-100 to create a 1% (w/w) solution within the PEG-salt ATPS significantly increased the time to phase separate.

The second ATPS whose lysing capabilities were studied was the 1:1 and 1:9 volume ratio Triton X-114 micellar ATPS. Like Triton X-100, Triton X-114 is a surfactant containing a hydrophobic tail that can poke holes into the cell membrane. Introduction of holes into the bilayer can cause intracellular components to leak out due to the osmotic pressure. In addition, as the membrane loses more rigidity, the osmotic pressure can cause lysis. At high enough concentrations, Triton X-114 may also completely solubilize the cell membrane, allowing more intracellular contents to be released, which ultimately leads to the same result as lysing cells.

Results of this experiment suggest that both types of the ATPSs successfully lyse cells, suggested by the protein that was released and subsequently quantified, in comparison to the PBS negative control (Figure 2.3.1). The 1% (w/w) Triton X-100 solution served as the positive control as this was the upper limit of Triton X-100 concentration recommended for use in lysis reagents. For $1x10^6$ HeLa cells, both volume ratios of the PEG-salt ATPS with Triton X-100 demonstrated the ability to lyse cells. These values are comparable to the amount extracted from commercially available lysis reagents on the market, whose protein yield ranges from approximately 160-200 μg of protein after an identical incubation time with the same amount of HeLa cells.[34] Additionally, it is interesting to note that both volume ratios of the Triton X-114 micellar ATPSs extracted more protein as compared to the PEG-salt ATPSs spiked with Triton X-100. This is because operating conditions that yield the 1:1 and 1:9 volume ratios result in a relatively high concentration of surfactant that is not conventionally required to lyse cells. Furthermore, the increase in protein mass may be due to the ability of micellar ATPSs to extract

hydrophobic membrane proteins, which is not as efficient in its recovery within a PEG-salt ATPS.

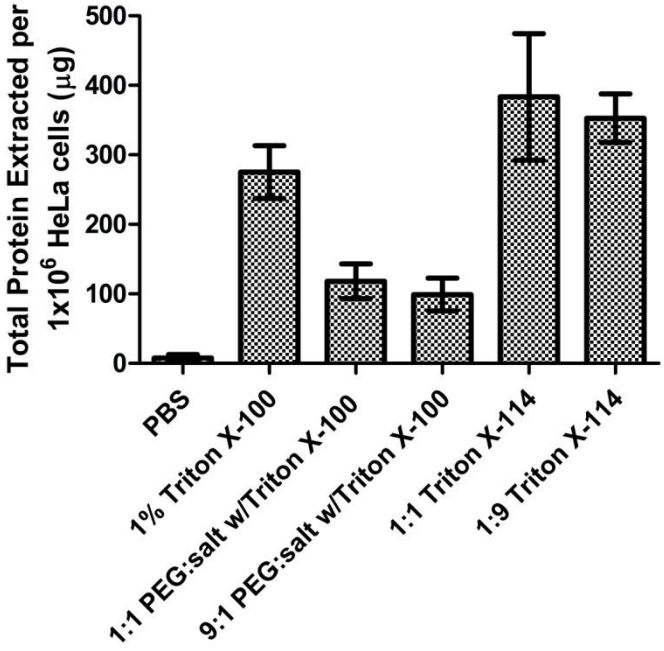

Figure 2.3.1 Total protein yield from various ATPS solutions (n=3). All solutions were incubated with $1x10^6$ HeLa cells for 5 min, clarified by centrifugation, and quantified using the BCA assay. PBS and 1% Triton X-100 serve as the negative and positive controls, respectively. Both types of ATPSs show the ability to lyse cells at both volume ratios. The Triton X-114 micellar ATPS solutions recovered more protein mass most likely due to its ability to extract membrane proteins.

Additionally, another method of quantifying the total protein extracted from lysis was performed for the Triton X-114 micellar ATPS. Here, an overnight incubation at 4°C was used for the Triton X-114 micellar ATPSs, as opposed to at room temperature for 2 hr (data reported in Figure 2.3.1). These results are compared to the room temperature experiments in Table 2.3.1, and they are comparable.

Table 2.3.1 Total Protein Recovery for Triton X-114 micellar ATPS

Volume Ratio	Method	**Protein extracted** (n=3)
1:1	2 hr at room temperature	383.35 ± 91.03 μg
	Overnight at 4°C	350.49 ± 21.38 μg
1:9	2 hr at room temperature	353.56 ± 34.99 μg
	Overnight at 4°C	331.19 ± 23.86 μg

2.3.2 Visualization of Accelerated ATPS Phase Separation on Paper

Previously, our laboratory discovered a new phenomenon that suggests that particular types of paper in addition to specific paper architecture can accelerate the rate of phase separation of an ATPS.[23,24] The use of a 3D paper well or 3D paper wick device demonstrated greater ATPS phase separation efficiency over a single paper membrane as it increased the cross-sectional area perpendicular to sample flow. Here, we confirm and identify the optimal conditions and 3D paper design required to achieve accelerated ATPS phase separation on paper for the 9:1 volume ratio PEG-salt ATPS with Triton X-100 and the 1:9 volume ratio Triton X-114 micellar ATPS.

Integration of ATPS with LFA as a means of concentrating a target biomolecule can improve the detection limit of traditional LFA tests and allow currently limited paper-based diagnostic devices to be successful in resource-poor settings. A diagnostic assay that integrates ATPS and LFA can be achieved by flowing both phases of the ATPS solution through the test strip such that the test and control line within the detection region is first exposed to the phase containing the concentrated biomolecule. In order to distinguish between the two phases of the ATPS as it wicks through paper, Brilliant Blue FCF dye and BSA-GNs were added for visualization of the typically colorless phases. This was important to observe how the ATPS flows on the paper, as it was critical in understanding its behavior and evaluating its performance.

For the PEG-salt ATPS with Triton X-100, the Brilliant Blue FCF dye partitions favorably to the top PEG-rich phase whereas the BSA-GNs, which appear dark red due to surface plasmon resonance[27], partition into the bottom salt-rich phase (Figure 2.3.2a). Since Brilliant Blue FCF is a small hydrophobic dye, it experiences minimal excluded-volume interactions, and partitions more favorably into the upper PEG-rich phase. In contrast, the larger and more hydrophilic BSA-GNs experience greater steric, excluded-volume interactions from the more hydrophobic PEG-rich phase on top, while their hydrophilicity further drives them toward the relatively hydrophilic salt-rich phase. Previously, the PEG-salt ATPS demonstrated accelerated phase separation on a 3D paper well comprised of layers of fiberglass paper.[23] However, this set up required the solution to be directly added on top of the 3D paper well using a pipette and then the addition of a running buffer to help collect and flush the salt-rich domains out of the paper well. This extra step is undesired and thus we investigated the use of a 3D paper wick for use with the PEG-salt ATPS with Triton X-100.

The 3D paper wick, which is designed to have the 3D portion of the paper vertically inserted into the ATPS sample solution, has also previously demonstrated the ability to significantly enhance phase separation for the Triton X-114 micellar ATPS system without the need to add a running buffer.[24] Use of the 3D paper wick with the micellar ATPS will be discussed shortly, however, we experienced difficulty in observing phase separation when using the more extreme volume ratios of the PEG-salt ATPS with Triton X-100. The addition of Triton X-100 into the ATPS was not expected to have been negatively affecting phase separation as the lack of enhanced phase separation was also observed for PEG-salt ATPSs without Triton X-100. Although the features of the fiberglass paper is hypothesized to allow for the PEG-rich and salt-rich domains to form and find each other more quickly, having the sample run vertically through

the 3D paper wick perhaps prevented the salt-rich domains from moving efficiently through the fiberglass paper matrix. This may be a result of having the more viscous PEG-rich domains that interact more favorably with the fiberglass paper, blocking and hindering the ability of salt-rich domains to move to the front of fluid flow. Additionally, these more viscous PEG-rich domains may have trouble wicking through paper vertically as it must flow against the force of gravity pushing down and affecting the capillary flow, further preventing the salt-rich domains to escape to the fluid front without the aid of a running buffer.

To address this problem, we found that treating the fiberglass paper with 0.1% (w/v) sodium cholate in PBS returned the ability of the PEG-salt ATPS with Triton X-100 to experience accelerated phase separation on paper (Figure 2.3.2b). Sodium cholate, otherwise known as cholic acid, is a trihydroxy bile salt which functions physiologically to allow absorption and digestion of dietary fats and oils by acting as a surfactant that emulsifies them into micelles. In the laboratory, it is used as a non-denaturing detergent for the extraction of membrane proteins. However, in our application, we hypothesized that treating the paper with a low concentration of sodium cholate acts to change the wetting properties of the paper to favorably allow salt-rich domains to more easily find each other, form channels through the other PEG-rich domains, and collect to the leading fluid front. Addition of a small amount of surfactant may be beneficial in the future to decrease the surface tension when dealing with cervical samples that may be viscous in nature after collection. Furthermore, it should be noted that treating the paper with higher concentrations of sodium cholate will lower the resulting volume ratio of the PEG-salt ATPS with Triton X-100. In addition to treating the fiberglass paper with 0.1% (w/v) sodium cholate, we recommend the use of an ATPS on a lower tie line,

reducing the viscosity of the homogenous ATPS to obtain a faster fluid wicking rate and consequently, more enhanced phase separation.

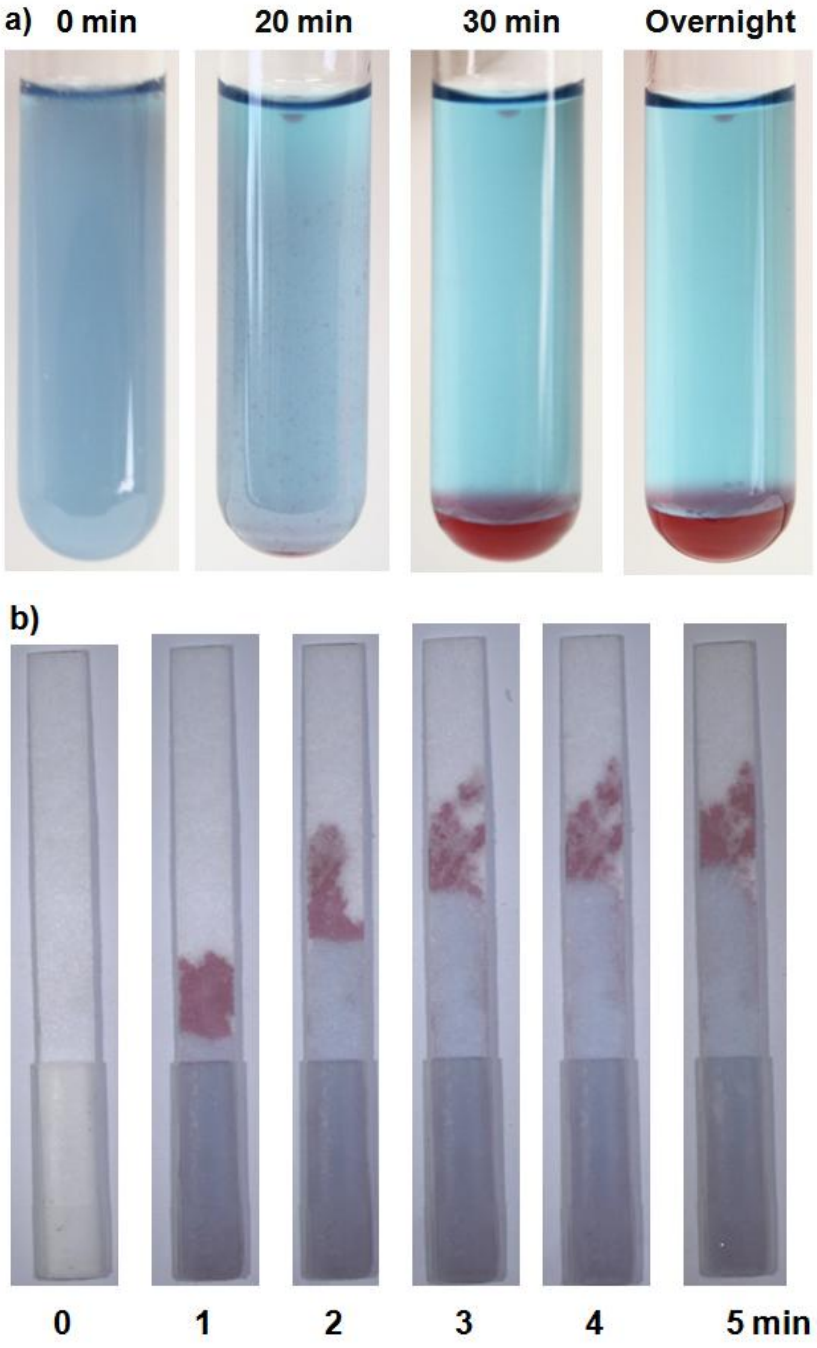

Figure 2.3.2 a) Phase separation of a 9:1 volume ratio PEG-salt ATPS with Triton X-100. Brilliant blue FCF dye and BSA-GNs have been added to visualize the top and bottom phases, respectively. b) Enhanced phase separation is observed on a 3D paper wick that has been treated with 0.1% sodium cholate. The PEG-rich domains (shown in blue) are hindered in the paper while the salt-rich domains (shown in dark red), which would contain concentrate target biomolecules, move ahead to lead the front of fluid flow.

Similarly, the Triton X-114 micellar ATPS demonstrated accelerated phase separation when applied onto fiberglass paper. When the Brilliant Blue FCF dye and BSA-GNs were added to this system, the Brilliant Blue FCF dye partitioned extremely into the bottom micelle-rich phase whereas the BSA-GNs partitioned into the top micelle-poor phase (Figure 2.3.3a). The partitioning behavior observed was due to reasons similar to those described for the PEG-salt ATPS with Triton X-100, taking into consideration the physico-chemical properties of the partitioning species. The small, hydrophobic Brilliant Blue FCF dye partitions extremely into the bottom, hydrophobic micelle-rich phase and the BSA-GNs partition favorably into the top, micelle-poor region where it will experience fewer steric, excluded-volume interactions from the large micelles in the micelle-rich phase.

The main benefit of incorporating the 3D paper wick into the Triton X-114 micellar ATPS is the ability to significantly shorten the time required to achieve phase separation. Typically, the Triton X-114 micellar ATPS requires a time scale on the order of hours to attain macroscopic phase separation equilibrium due to the small density difference and small interfacial tension between the micelle-rich and micelle-poor domains. Additionally, when the top phase shrinks with more extreme volume ratios, this phase separation time increases as the microscopic micelle-poor domains of the micelle-poor phase have more difficulty finding each other. However, when a homogeneous Triton X-114 micellar ATPS is applied onto the 3D wick, phase separation is observed to occur on the order of minutes (Figure 2.3.3b).

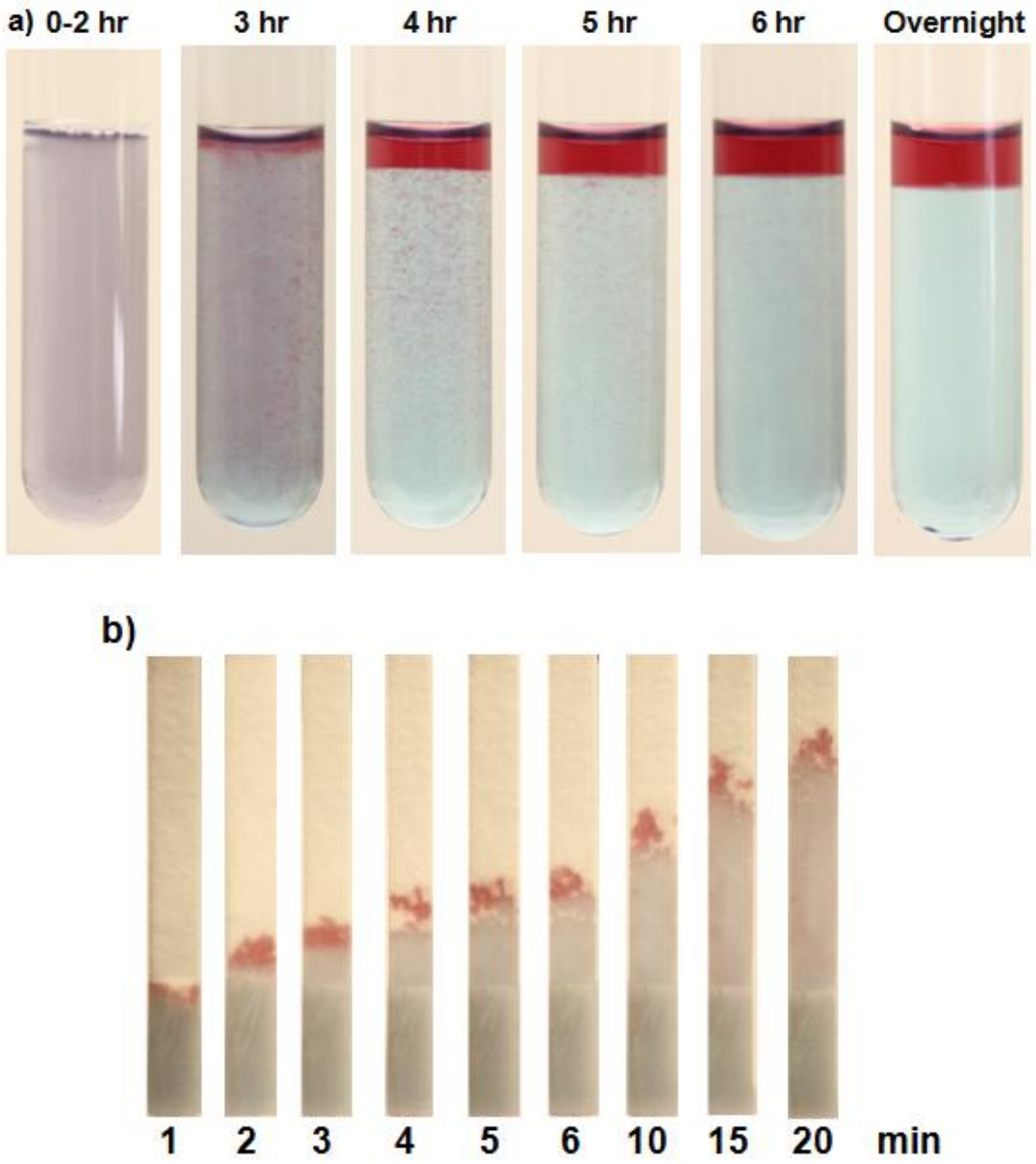

Figure 2.3.3 a) Phase separation of a 1:9 volume ratio Triton X-114 micellar ATPS solution. Brilliant Blue FCF dye and BSA-GNs were added to visualize the bottom and top phases, respectively. Thermodynamic equilibrium is achieved on order of hours. b) The same 1:9 volume ratio Triton X-114 micellar ATPS demonstrates enhanced phase separation as it wicks through a 3D paper wick. This significantly speeds up phase separation from hours to minutes. Note that the punctate appearance of the fluid front is due to the domains traveling through the pores of the fiberglass paper (beneath the top surface), which may be difficult to visualize when the domains do not wick through the top of the paper strip.

2.3.3 Determining Partition Coefficients

After confirming that the ATPSs can lyse HeLa cells and experience accelerated phase separation on paper, we performed partitioning studies with a model particle in our ATPS systems. The HPV capsid is comprised of 360 copies of the major capsid protein L1 and exhibits T=7 icosahedral symmetry formed from the interaction among 72 pentamers of L1. Minor capsid protein L2 associates with the L1 pentamers, although the structural relationship of L2 to L1 within the capsid is unknown.[35] The virus is found to be around 50-60 nm in diameter.[25]

Here, we were interested in studying how a particle of similar size will partition in our ATPS solutions in addition to studying how the effect of hydrophilicity/hydrophobicity of a particle would affect its partitioning. It is well accepted that several factors influence partitioning, such as concentrations of phase-forming components, molecular weight of polymers, temperature, pH, and solute charge, in addition to size and hydrophobicity of the particle. As such, hydrophobic 50 nm green fluorescent polystyrene beads and more hydrophilic radiolabeled DGNPs (~ 50 nm in diameter as measured by dynamic light scattering) were chosen as our model particles. These particles were placed in a 1:1 volume ratio PEG-salt ATPS with Triton X-100 as well as a 1:1 volume ratio Triton X-114 micellar ATPS.

To quantify the partitioning behavior of the particles in the ATPSs, the partition coefficient K was determined, and it is defined as follows:

$$K \equiv \frac{C_{p,top}}{C_{p,bottom}} \qquad (1)$$

Where $C_{p,top}$ and $C_{p,bottom}$ are the concentrations of the particle in the top and bottom phases, respectively. The polystyrene beads were observed to partition to the bottom, micelle-rich phase for the Triton X-114 micellar ATPS and partition to the interface of the PEG-salt ATPS with

Triton X-100. Since these particles did not distinctly partition into one of the two phases for the PEG-salt ATPS with Triton X-100, this system was not ideal to continue to use for partitioning experiments. Therefore, the radiolabeled DGNPs were only added to the Triton X-114 micellar ATPS. The calculated partition coefficients are shown below in Table 2.3.2.

Table 2.3.2 Experimental Partition Coefficients

1:1 volume ratio Triton X-114 micellar ATPS	
Particle (50 nm)	***K*** (n=3)
Polystyrene	0.77 ± 0.07
DGNPs	10.5 ± 1.1

A partition coefficient that is greater than 1 indicates that particles partition favorably into the top phase, whereas a partition coefficient that is less than 1 indicates that particles partition favorably into the bottom phase. Accordingly, a partition coefficient equal to 1 means that the particle partitions evenly between the two phases of the ATPS. For the polystyrene nanoparticle, $K = 0.77 \pm 0.07$, suggesting that the particles slightly favor the bottom phase of the Triton X-114 micellar ATPS. Here, the competition between hydrophobic interactions and excluded-volume interactions was evident as the particles do not partition extremely into a single phase, and rather, somewhat evenly into both phases. The hydrophobicity of the polystyrene beads tends to drive the particles down to the more hydrophobic, micelle-rich phase. However, the relatively large size of the 50 nm particle contributed to the particle favoring the top, micelle-poor phase where it will experience fewer steric, excluded-volume interactions with the less abundant micelles.

However, this was not the case for the hydrophilic DGNPs with a $K = 10.5 \pm 1.1$, demonstrating that these particles prefer to reside in the top, micelle-poor phase. This contrast

was expected as the DGNPs will not only favor the relatively more hydrophilic top phase, but also experience steric exclusion from the more abundant micelles in the bottom phase.

2.3.4 Predicting Partition Coefficients using Thermodynamics

Since it is clear that physico-chemical properties of nanoparticles play a role in the partitioning behavior of that particle, we now aimed to create an initial model that can reasonably predict the partition coefficient of a spherical particle within the Triton X-114 micellar ATPS based on its size and hydrophobicity. We chose to focus on this specific ATPS as the polystyrene particles that were studied within the PEG-salt ATPS with Triton X-100 visually partitioned to the interface between the top and bottom phases, a behavior that will not be captured by this model.

To begin, at thermodynamic equilibrium, the chemical potential of the particle in the top phase is equal to the chemical potential of the particle in the bottom phase as the particle is allowed to freely diffuse between both phases. Thus, this diffusional equilibrium of the model particle can be described as follows:

$$\mu_{p,top} = \mu_{p,bottom} \tag{2}$$

where $\mu_{p,top}$ and $\mu_{p,bottom}$ are the chemical potentials of the particle in the top and bottom phases, respectively. The chemical potentials in the top and bottom phases can also be written as follows:

$$\mu_{p,top} = \mu_p^\circ + k_B T \ln C_{p,top} + \mu_{p,top}^{ex} \tag{3}$$

$$\mu_{p,bottom} = \mu_p^\circ + k_B T \ln C_{p,bottom} + \mu_{p,bottom}^{ex} \tag{4}$$

where μ_p° is the 1 molecule/mL standard state for the particle, k_B is the Boltzmann constant, *T* is the absolute temperature in Kelvins, $C_{p,top}$ and $C_{p,bottom}$ are the concentrations of the particles in units of molecules/mL in the top and bottom phases, respectively, and $\mu_{p,top}^{ex}$ and $\mu_{p,bottom}^{ex}$ are the excess chemical potentials of the particle in the top and bottom phases, respectively. Substitution of Eqs. (3) and (4) into Eq. (2), followed by rearrangement of terms yields:

$$\frac{C_{p,top}}{C_{p,bottom}} = \exp\left[\frac{-(\mu_{p,top}^{ex} - \mu_{p,bottom}^{ex})}{k_B T}\right] \tag{5}$$

From the definition of partition coefficient *K* as defined in Eq. (1), Eq. (5) can be rewritten as:

$$K = \exp\left[\frac{-(\mu_{p,top}^{ex} - \mu_{p,bottom}^{ex})}{k_B T}\right] \tag{6}$$

Based on Eq. (6), the partitioning behavior of the particle is governed by differences between its excess chemical potentials in the top and bottom phases. The excess chemical potential of the particle in phase α can be obtained using the following equation:

$$\mu_{p,\alpha}^{ex} = \left(\frac{\partial G_\alpha^{ex}}{\partial N_{p,\alpha}}\right)_{T,P,\mathrm{N}_{j\neq p,\alpha}} \tag{7}$$

where G_α^{ex} is the excess Gibbs free energy of phase α, $N_{p,\alpha}$ is the number of particles in phase α, $N_{j\neq p,\alpha}$ is the number of molecules of type *j* (not corresponding to the particle) in phase α, and *T* and *P* are the absolute temperature and pressure in the coexisting phases, respectively.

In an aqueous two-phase nonionic micellar system, the excess Gibbs free energy in phase α can be approximated as follows:

$$G_\alpha^{ex} = G_\alpha^{ex,EV} + G_\alpha^{ex,h\phi} \tag{8}$$

where $G_\alpha^{ex,EV}$ is the contribution to the excess Gibbs free energy in phase α due to excluded-volume interactions and $G_\alpha^{ex,h\phi}$ is the contribution due to hydrophobic interactions. The contribution due to other types of interactions, such as electrostatic or van der Waals, are assumed to be negligible. Incorporating Eqs. (7) and (8) into Eq. (6) yields the following:

$$K = \exp\left[\frac{-(\mu_{p,top}^{ex,EV} - \mu_{p,bottom}^{ex,EV})}{k_B T}\right] \cdot \exp\left[\frac{-(\mu_{p,top}^{ex,h\phi} - \mu_{p,bottom}^{ex,h\phi})}{k_B T}\right] \tag{9}$$

where $\mu_{p,top}^{ex,EV}$ and $\mu_{p,bottom}^{ex,EV}$ are the excess chemical potentials of the particle when considering excluded-volume interactions in the top and bottom phases, respectively, and $\mu_{p,top}^{ex,h\phi}$ and $\mu_{p,bottom}^{ex,h\phi}$ are the excess chemical potential of the particle due to hydrophobic interactions in the top and bottom phases, respectively. From Eq. (9), we see that the contributions from excluded-volume and hydrophobic interactions to the overall partition coefficient can be written as:

$$K = K_p^{EV} K_p^{h\phi} \tag{10}$$

where K_p^{EV} and $K_p^{h\phi}$ represent the contribution of excluded-volume interactions and hydrophobic interactions to *K*, respectively.

Accordingly, the first term in Eq. (10) can be reasonably predicted using the following expression derived from Blankschtein and coworkers[36]:

$$K_p^{EV} = \exp\left[-(\phi_t - \phi_b)\left(1 + \frac{R_s}{R_0}\right)^2\right] \tag{11}$$

where ϕ_t and ϕ_b are the surfactant volume fractions in the top and bottom phases, respectively, R_s is the hydrodynamic radius of a spherical molecule, and R_0 is the cross-sectional radius of each cylindrical micelle. This expression was derived considering only the repulsive, steric, excluded-volume interactions that operate between the spherical nanoparticles and the cylindrical micelles.

In Eq. (11), the difference between ϕ_t and ϕ_b was estimated by assuming that the density of the top and bottom phases are approximately equal to 1 g/mL which transforms the $\phi_t - \phi_b$ term into a weight fraction difference rather than a volume fraction difference. Accordingly, $\phi_t - \phi_b$ can alternatively be viewed as the tie-line length. The weight fraction difference between the top and bottom phases of a 4% Triton X-114 micellar ATPS at 25°C after phase separation is approximately -0.06 after visualization of the tie-line length of a coexistence curve of Triton X-114.[37] The value for R_s was 250 Å, as the diameter of the monodisperse spherical polystyrene nanoparticles was 50 nm, and R_0 of the micelles was 23.4 Å.[37] Plugging these literature values into Eq. (11) yields K_p^{EV} as equal to 3.607 x 10^3.

With regard to the hydrophobic contribution, the $K_p^{h\phi}$ was estimated using the octanol-water partition coefficient (K_{OW}) of styrene, which is the repeating monomeric unit within the polystyrene beads. The octanol-water partition coefficient describes the partitioning of a species between an octanol-water two phase system where the top hydrophobic phase is comprised of the less dense octanol and the bottom phase is comprised of water. Therefore, the inverse of the K_{OW} value of styrene will be used to estimate the partition coefficient of the polystyrene particle in the Triton X-114 micellar ATPS solution, where the more hydrophobic phase is on the bottom. K_{OW} of styrene is 1.445 x 10^3 and thus $K_p^{h\phi}$ is approximately 1/(1.445 x 10^3).[38] Plugging all

determined values into Eq. (10) gives an overall partition coefficient of 2.5, for the partitioning of 50 nm polystyrene beads within the Triton X-114 micellar ATPS, which is reasonable compared to the experimental value of 0.77.

2.4 Conclusion

This chapter focused on investigating two types of ATPSs, the PEG-salt ATPS with Triton X-100 as well as the Triton X-114 micellar system. Here we demonstrate that both ATPS solutions can lyse HeLa cells effectively within 5 mins as measured by the release of protein. Additionally, we observed accelerated phase separation of both ATPSs on 3D paper architectures under optimized conditions. Specifically, it was discovered that the fiberglass paper needed to be treated with sodium cholate to allow the PEG-salt ATPS with Triton X-100 to exhibit enhanced phase separation on the 3D paper wick structure. We hypothesized that at low concentrations, the surfactant characteristics of sodium cholate favorably altered the wetting properties of the paper to allow the salt-rich domains to wick vertically and more efficiently through the fiberglass membranes.

After confirming that both ATPS solutions exhibited the desired cell lysis and phase separation properties, the partitioning of model hydrophilic and hydrophobic particles was studied. A mathematical model was developed based on thermodynamic principles and considered contributions from excluded-volume and hydrophobic interactions to predict partition coefficients of a particle in a Triton X-114 micellar ATPS. The model reasonably predicted the measured partition coefficient value, and therefore, can be further developed in the future to provide even more accurate predictions of partition coefficients.

3: Detecting HPV16 L1 Major Capsid Protein using the Lateral-Flow Immunoassay (LFA)

3.1 Motivation and background

Effective prevention and treatment of cervical cancer in women is heavily dependent on regular screenings as well as early and accurate diagnosis. Additionally, the advent of prophylactic HPV vaccines has significantly reduced the risk for cervical cancer development. Yet, cervical cancer remains a leading cause of cancer-related death for women in low income countries due to several barriers, including minimal cervical cancer screening programs, limited number of health care professionals, and inadequate access to gold-standard screening technologies. The continued global burden of cervical cancer thus motivates the need for alternative screening approaches that can address the challenges in resource-poor settings.

For this reason, women in resource-poor communities could greatly benefit from a simple, low-cost, and equipment-free test that can be self-administered and can quickly provide easily interpretable results. One diagnostic assay that satisfies these criteria is the lateral-flow immunoassay (LFA) which is an affordable, user-friendly, and portable paper-based diagnostic device. In this chapter, the limit of detection of HPV16 L1 was determined with LFA only, which suggests that the sensitivity of this test can further be enhanced upon integration with ATPS. Additionally, to our knowledge, this is the first successful demonstration of detection of the HPV16 L1 major capsid protein using LFA.

3.1.1 Lateral-Flow Immunoassay (LFA)

The lateral-flow immunoassay (LFA) is an antibody-based assay that can rapidly detect for the presence or absence of a desired biomarker by utilizing colorimetric indicators, such as colloidal gold nanoparticles (GNs) conjugated with specific antibodies against the analyte, as the

sample travels through the test strip via capillary flow. A typical LFA test strip is comprised of three main components: a sample pad, membrane, and absorbent pad (Figure 3.1.1). The upstream end of the test strip begins with the sample pad where the sample is applied and allowed to wick through the remainder of the test strip. Directly after the sample pad is the membrane where detection of the biomarkers occurs. This is achieved by immobilizing antibodies on the membrane to capture the target molecule. Lastly, the furthest downstream end of the test strip consists of the absorbent pad which maintains flow of the sample through the entirety of the test strip by acting as a reservoir to absorb excess liquid. Marketed LFA tests additionally have a conjugate pad dried with the colorimetric indicator targeted against the analyte which releases these nanoparticles as the pad is rehydrated. The conjugate pad is therefore placed between the sample pad and membrane. Since the components of the LFA test strip tend to be thin and fragile, they are typically placed on an adhesive vinyl backing and often housed in a plastic encasing where the sample pad is exposed and a reading window is visible.

Some common applications of LFA include the detection of viral pathogens, drugs, hormones, or biotoxins. However, the most well-known application of LFA is the over-the-counter pregnancy test. LFAs are suitable for use at the POC as they are portable, equipment-free, light in weight, low-cost, user-friendly, and require minimal power or electricity to operate.

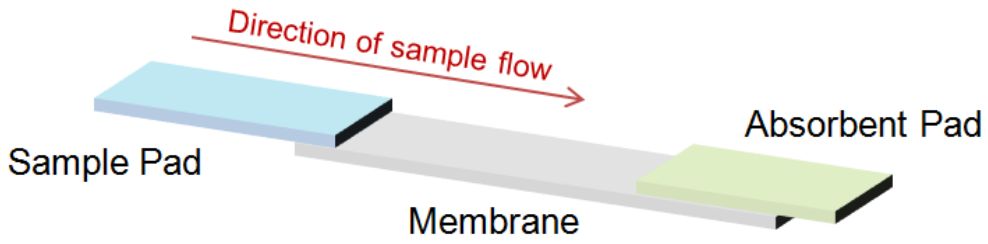

Figure 3.1.1 Schematic representation of an LFA strip. The sample pad is shown in blue, the membrane is shown in grey, and the absorbent pad is shown in green.

3.1.2 Sandwich Assay Format

LFA comes in two assay formats, the competitive assay format and the sandwich assay format. For detecting larger analytes with multiple antibody binding domains, such as HPV, the sandwich assay format is utilized. In this format, colloidal gold nanoparticles used for this test are conjugated with primary antibodies against the target biomolecule to form gold nanoprobes (GNPs). Antibodies against the target are also printed across the membrane to form the test line. These primary antibodies immobilized on the test line may either be the same or different antibodies on the GNPs; the selection of these primary antibodies is typically chosen in order to optimize the resulting test line intensity for specific applications. The control line, which lies downstream of the test line, is made up of a secondary antibody against the primary antibody on the GNPs.

A positive test in the sandwich assay format is indicated by the presence of two lines, a visible band across both the test line and control line. Since samples in LFA come into contact with the GNPs prior to the test and control lines, the presence of a target biomolecule will allow the GNPs to bind to the target first. Subsequently, as the sample travels up the membrane, the primary antibodies immobilized on the test line will bind to the target biomolecule-GNP complex, resulting in the target analyte being “sandwiched” between the primary antibodies on

the test line and the GNPs. These "sandwiched" complexes are responsible for the visible band formed at the test line, indicating a positive result. The presence of a visible band at the control line indicates a valid test as it demonstrates that the sample has traveled through the entire test strip since the secondary antibodies on the control line have bound to the primary antibodies on the remaining GNPs. On the other hand, a negative test is determined by the presence of solely the control line, as lack of the biomarker only allows freely floating GNPs to bind to the control line. The sandwich assay mechanism is depicted in Figure 3.1.2. Results from the LFA in sandwich assay format are typically intuitive to end-users as negative results are denoted by the presence of one visible band while positive results are denoted by seeing two red bands.

In this case, the test line intensity for the sandwich assay is proportional to the amount of target analyte in the sample. Very low concentrations of the analyte can yield false negative results because there is not enough of the biomarker that can be sandwiched at the test line for a test line to appear. Therefore, the lowest biomarker concentration that must be available to give a true positive test result is defined as the detection limit, or limit of detection. Unfortunately, LFA has limited applicability as its sensitivity is inferior to that of gold-standard laboratory assays when biomarkers are present at low concentrations. This problem can be addressed by pre-concentrating the targets in a sample prior to detection with LFA.

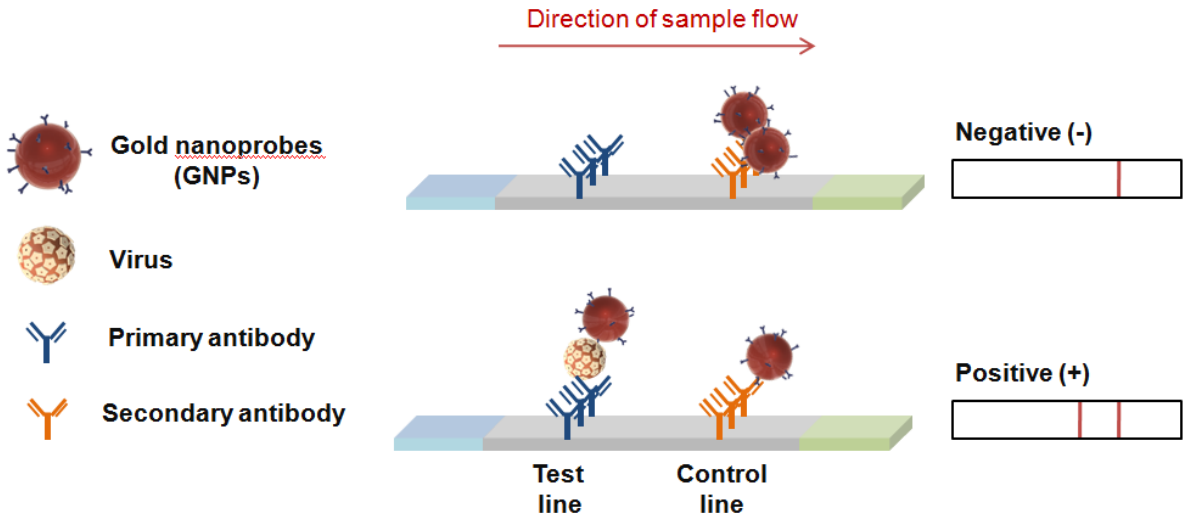

Figure 3.1.2 Schematic representation of negative and positive LFA test results using the sandwich assay mechanism to detect for a presence of a model virus. The absence of the virus yields a negative test, denoted by a single visible band at the control line. A positive test results in two visible bands at the test and control lines, as the virus is "sandwiched" at the test line, forming a complex between the primary antibodies on the test line and nanoprobes.

3.2 Materials and Methods

3.2.1 Preparation of Anti-HPV16 L1 Colloidal Gold Nanoprobes (GNPs)

Gold nanoprobes (GNPs) targeted against the major capsid protein L1 of HPV16 were prepared from gold nanoparticles whose synthesis was described in Chapter 2. To begin, the pH of 1 mL of the gold nanoparticles was adjusted to a pH of approximately 7.0-8.0 by adding 60 µL of 0.1 M sodium borate. Subsequently, 8 µg of mouse monoclonal anti-HPV16 L1 antibody (MyBioSource, San Diego, CA), were added and the solution was mixed for 30 min on a shaker to facilitate the formation of dative bonds between the antibodies and the gold nanoparticles. Subsequently, 200 µL of 10% (w/v) BSA solution were added to stabilize the gold nanoparticles by preventing the nonspecific binding of other proteins onto its surface, and the suspension was incubated on the shaker for another 15 min. Free antibodies were removed by centrifuging the

mixture for 30 min at 11,000 rpm and the pellet, containing functionalized GNPs, was isolated and resuspended in 200 μL of 1% (w/v) BSA in water. Centrifugation and resuspension of the resulting pellet was repeated twice more and the final pellet was resuspended in 100 μL of 0.1 M sodium borate buffer at pH 9.0.

3.2.2 Assembling LFA Strips

The sandwich assay format was used for this particular LFA test strip. An anti-HPV16 L1 antibody concentration of 0.6 mg/mL was printed as test line and a concentration of 0.3 mg/mL goat-x-mouse anti-IgG (Bethyl Laboratories, Montgomery, TX) for the control line on nitrocellulose membrane (Sartorius, Göttingen, Germany). The membranes were then vacuum-dried in a dessicator overnight. Subsequently, portions of the membrane were soaked in a solution of 5% (w/v) sucrose, 0.1% (w/v) Tween, 1% BSA (w/v) in borate buffered saline (BBS, 150 mM sodium borate, 25 mM sodium chloride) for one hour. Excess solution was then blotted off the membrane and the membrane was put under a low pressure vacuum overnight. The purpose of blocking this membrane with the aforementioned buffer is to improve fluid flow and prevent nonspecific binding to the test line. The nitrocellulose membranes were then removed and placed in a container with packages of desiccant for long term storage.

To assemble the full LFA test strip, the membranes were placed on an adhesive backing with a cellulose absorbent pad (Whatman Intl, Maidstone, England) placed upstream and a fiberglass sample pad placed downstream. Prior to placement on the adhesive backing, the sample pad was treated with 1% BSA in water and put under a low pressure vacuum to dry the fiberglass paper.

3.2.3 Detection of HPV16 L1

The detection limit of the L1 virus like particle (VLP) was determined with LFA. The sample suspension consisted of 15 μL of a known amount of L1 in PBS and 5 μL of anti-HPV16 L1 GNPs. LFA test strips were inserted vertically such that the sample pad was able to collect the sample. Subsequently, 30 μL of running buffer (0.2% (w/v) BSA, 0.3% Tween 20, 0.2% sodium azide, 0.1% PEG in 0.1M Trizma base, pH 8.0) were added to ensure the entire sample traveled through the LFA test strip. Images were captured after 20 min.

3.3 Results and Discussion: Detection of Major Capsid Protein L1 with LFA

Although we would like to eventually use the Triton X-114 micellar ATPS to preconcentrate HPV16, the first main goal of developing a POC device for cervical cancer screening is to investigate whether it is even feasible to detect the desired biomarker using LFA. The biomarker of interest is the major capsid protein L1, and studies have shown that L1 self assembles into virus-like particles (VLPs) even in the absence of L2. The L1 VLPs are assemblies of approximately 72 L1 pentamers in a shell similar to that of the virion, however, when L1 is crystallized, conditions favor the formation of a 12-pentamer, T=1 icosahedral small VLP.[39] Therefore, L1 itself should be able to detected by the LFA in sandwich assay format as there are still multiple antibody binding sites available for the L1 VLP to be "sandwiched" by the anti-HPV16 L1 GNPs and the antibodies immobilized on the test line.

We first opted to target the major capsid protein L1 of HPV16, as this high-risk HPV has the strongest risk for cervical cancer development. Results of our LFA experiment demonstrated the ability of the LFA technology to detect for L1 VLPs, which should be able to be translated to detection of the HPV16 virus itself. Additionally, the LFA test strip was treated to reduce the incidence of nonspecific binding of the anti-HPV16 L1 GNPs which could potentially result in

false positives as GNPs complexes that have aggregated due to high protein content can nonspecifically bind at the test line. To prevent nonspecific binding, both the sample pad and membrane of the LFA test strip were treated. The sample pad was blocked with 1% (w/v) BSA in water. The nitrocellulose membrane was pretreated with a cocktail of other components, which include Tween 20, sucrose, and BSA in borate buffered saline (BBS).

With this preliminary set-up, the LFA test strip exhibited a limit of detection of 20 ng/μL of L1 (Figure 3.3.1). To reiterate, a positive result is indicated by the presence of two visible bands. As shown in Figure 3.3.1, the lowest concentration of L1 that could be detected in this preliminary experiment was 20 ng/μL as lower concentrations of L1 yielded false negative results. Future work will involve further optimizing this set up and combining it with the Triton X-114 micellar ATPS described in Chapter 2 to demonstrate an improvement in the detection limit.

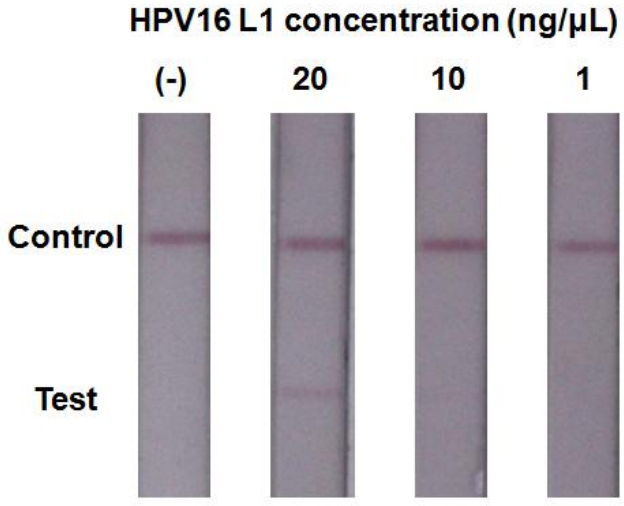

Figure 3.3.1 Detection of HPV16 L1 with LFA. This preliminary experiment demonstrates that LFA in sandwich assay format can successfully detect for the L1 major capsid protein on HPV16 with a limit of detection at 20 ng/μL prior to receiving false negative results.

3.4 Conclusion

HPV16 L1 VLPs were successfully detected at a detection limit of 20 ng/μL using LFA in sandwich assay format. These results may be further improved in the future through optimization of the LFA test strip set up as well as by incorporation of the Triton X-114 micellar ATPS system studied within this thesis.

The results provided in the current study demonstrate the potential to further develop this technology to create an end-user friendly POC device for cervical cancer screening. This is necessary as much of the disease burden lies within low income countries, motivating the need to create alternative screening options for women in resource-poor communities. In the future, when ATPS is integrated with LFA for the detection of the L1 major capsid protein of HPV16, the sensitivity of LFA may be enhanced to allow for the creation of a device that can rapidly assess cervical cancer risk in women, ultimately improving disease management and patient outcomes.

References

(1) Ferlay, J.; Soerjomataram, I.; Dikshit, R.; Eser, S.; Mathers, C.; Rebelo, M.; Parkin, D. M.; Forman, D.; Bray, F. Cancer Incidence and Mortality Worldwide: Sources, Methods and Major Patterns in GLOBOCAN 2012. *Int. J. Cancer* **2015**, *136* (5), E359–E386.

(2) WHO | Human Papillomavirus (HPV) and Cervical Cancer.

(3) Peirson, L.; Fitzpatrick-Lewis, D.; Ciliska, D.; Warren, R. Screening for Cervical Cancer: A Systematic Review and Meta-Analysis. *Syst. Rev.* **2013**, *2*, 35.

(4) Walboomers, J. M.; Jacobs, M. V; Manos, M. M.; Bosch, F. X.; Kummer, J. A.; Shah, K. V; Snijders, P. J.; Peto, J.; Meijer, C. J.; Muñoz, N. Human Papillomavirus Is a Necessary Cause of Invasive Cervical Cancer Worldwide. *J. Pathol.* **1999**, *189* (1), 12–19.

(5) Clifford, G. M.; Smith, J. S.; Plummer, M.; Muñoz, N.; Franceschi, S. Human Papillomavirus Types in Invasive Cervical Cancer Worldwide: A Meta-Analysis. *Br. J. Cancer* **2003**, *88* (1), 63–73.

(6) Giuliano, A. R.; Harris, R.; Sedjo, R. L.; Baldwin, S.; Roe, D.; Papenfuss, M. R.; Abrahamsen, M.; Inserra, P.; Olvera, S.; Hatch, K. Incidence, Prevalence, and Clearance of Type- Specific Human Papillomavirus Infections: The Young Women's Health Study. *J. Infect. Dis.* **2002**, *186* (4), 462–469.

(7) Stanley, M. Immune Responses to Human Papillomavirus. *Vaccine* **2006**, *24*, S16–S22.

(8) Doorbar, J.; Quint, W.; Banks, L.; Bravo, I. G.; Stoler, M.; Broker, T. R.; Stanley, M. A. The Biology and Life-Cycle of Human Papillomaviruses. *Vaccine* **2012**, *30*, F55–F70.

(9) Schiffman, M.; Castle, P. E.; Jeronimo, J.; Rodriguez, A. C.; Wacholder, S. Human Papillomavirus and Cervical Cancer. *Lancet* **2007**, *370* (9590), 890–907.

(10) Thomas, M.; Pim, D.; Banks, L. The Role of the E6-p53 Interaction in the Molecular

Pathogenesis of HPV. *Oncogene* **1999**, *18* (53), 7690–7700.

(11) Burd, E. M. Human Papillomavirus and Cervical Cancer. *Clin. Microbiol. Rev.* **2003**, *16* (1), 1–17.

(12) Woodman, C. B. J.; Collins, S. I.; Young, L. S. The Natural History of Cervical HPV Infection: Unresolved Issues. *Nat. Rev. Cancer* **2007**, *7*.

(13) Practice Bulletin No. 157. *Obstet. Gynecol.* **2016**, *127* (1), e1–e20.

(14) Solomon, D.; Davey, D.; Kurman, R.; Moriarty, A.; O'Connor, D.; Prey, M.; Raab, S.; Sherman, M.; Wilbur, D.; Wright, T.; Young, N.; Workshop, for the F. G. M. and the B. 2001. The 2001 Bethesda System. *J. Am. Med. Assoc.* **2002**, *287* (16), 2114–2119.

(15) Whitlock, E. P.; Vesco, K. K.; Eder, M.; Lin, J. S.; Senger, C. A.; Burda, B. U. Liquid-Based Cytology and Human Papillomavirus Testing to Screen for Cervical Cancer: A Systematic Review for the U.S. Preventive Services Task Force. *Ann. Intern. Med.* **2011**, *155* (10), 687–697, W214–W215.

(16) Wentzensen, N. HPV mRNA and p16 Detection as Biomarkers for the Improved Diagnosis of Cervical Neoplasia. **2008**, *17* (10), 2536–2545.

(17) Zhao, F.-H.; Jeronimo, J.; Qiao, Y.-L.; Schweizer, J.; Chen, W.; Valdez, M.; Lu, P.; Zhang, X.; Kang, L.-N.; Bansil, P.; Paul, P.; Mahoney, C.; Berard-Bergery, M.; Bai, P.; Peck, R.; Li, J.; Chen, F.; Stoler, M. H.; Castle, P. E. An Evaluation of Novel, Lower-Cost Molecular Screening Tests for Human Papillomavirus in Rural China. *Cancer Prev. Res.* **2013**, *6* (9), 938–948.

(18) Valdez, M.; Jeronimo, J.; Bansil, P.; Qiao, Y.-L.; Zhao, F.-H.; Chen, W.; Zhang, X.; Kang, L.-N.; Paul, P.; Bai, P.; Peck, R.; Li, J.; Chen, F.; Stoler, M. H.; Castle, P. E. Effectiveness of Novel, Lower Cost Molecular Human Papillomavirus-Based Tests for

Cervical Cancer Screening in Rural China. *Int. J. Cancer* **2016**, *138* (6), 1453–1461.

(19) Mashayekhi, F.; Chiu, R. Y. T.; Le, A. M.; Chao, F. C.; Wu, B. M.; Kamei, D. T. Enhancing the Lateral-Flow Immunoassay for Viral Detection Using an Aqueous Two-Phase Micellar System. *Anal. Bioanal. Chem.* **2010**, *398* (7-8), 2955–2961.

(20) Mashayekhi, F.; Le, A. M.; Nafisi, P. M.; Wu, B. M.; Kamei, D. T. Enhancing the Lateral-Flow Immunoassay for Detection of Proteins Using an Aqueous Two-Phase Micellar System. *Anal. Bioanal. Chem.* **2012**, *404* (6-7), 2057–2066.

(21) Jue, E.; Yamanishi, C. D.; Chiu, R. Y. T.; Wu, B. M.; Kamei, D. T. Using an Aqueous Two-Phase Polymer-Salt System to Rapidly Concentrate Viruses for Improving the Detection Limit of the Lateral-Flow Immunoassay. *Biotechnol. Bioeng.* **2014**, *111* (12), 2499–2507.

(22) Chiu, R. Y. T.; Nguyen, P. T.; Wang, J.; Jue, E.; Wu, B. M.; Kamei, D. T. Dextran-Coated Gold Nanoprobes for the Concentration and Detection of Protein Biomarkers. *Ann. Biomed. Eng.* **2014**, *42* (11), 2322–2332.

(23) Chiu, R. Y. T.; Jue, E.; Yip, A. T.; Berg, A. R.; Wang, S. J.; Kivnick, A. R.; Nguyen, P. T.; Kamei, D. T. Simultaneous Concentration and Detection of Biomarkers on Paper. *Lab Chip* **2014**, *14* (16), 3021.

(24) Pereira, D. Y.; Chiu, R. Y. T.; Zhang, S. C. L.; Wu, B. M.; Kamei, D. T. Single-Step, Paper-Based Concentration and Detection of a Malaria Biomarker. *Anal. Chim. Acta* **2015**, *882*, 83–89.

(25) Conway, M. J.; Meyers, C. Replication and Assembly of Human Papillomaviruses. *J. Dent. Res.* **2009**, *88* (4), 307–317.

(26) Smith, P. K.; Krohn, R. I.; Hermanson, G. T.; Mallia, A. K.; Gartner, F. H.; Provenzano,

M. D.; Fujimoto, E. K.; Goeke, N. M.; Olson, B. J.; Klenk, D. C. Measurement of Protein Using Bicinchoninic Acid. *Anal. Biochem.* **1985**, *150* (1), 76–85.

(27) Njoki, P. N.; Lim, I.-I. S.; Mott, D.; Park, H.-Y.; Khan, B.; Mishra, S.; Sujakumar, R.; Luo, J.; Zhong, C.-J. Size Correlation of Optical and Spectroscopic Properties for Gold Nanoparticles. *J. Phys. Chem. C* **2007**, *111* (40), 14664–14669.

(28) Frens, G. Particle Size and Sol Stability in Metal Colloids. *colloid Polym. Sci.* **1972**, *250* (7), 736–741.

(29) Jang, H.; Ryoo, S.-R.; Kostarelos, K.; Han, S. W.; Min, D.-H. The Effective Nuclear Delivery of Doxorubicin from Dextran-Coated Gold Nanoparticles Larger than Nuclear Pores. *Biomaterials* **2013**, *34* (13), 3503–3510.

(30) Scholzen, T.; Gerdes, J. The Ki-67 Protein: From the Known and the Unknown. *J. Cell. Physiol.* **2000**, *182* (3), 311–322.

(31) Petry, K. U.; Schmidt, D.; Scherbring, S.; Luyten, A.; Reinecke-Lüthge, A.; Bergeron, C.; Kommoss, F.; Löning, T.; Ordi, J.; Regauer, S.; Ridder, R. Triaging Pap Cytology Negative, HPV Positive Cervical Cancer Screening Results with p16/Ki-67 Dual-Stained Cytology. *Gynecol. Oncol.* **2011**, *121* (3), 505–509.

(32) Ikenberg, H.; Bergeron, C.; Schmidt, D.; Griesser, H.; Alameda, F.; Angeloni, C.; Bogers, J.; Dachez, R.; Denton, K.; Hariri, J.; Keller, T.; von Knebel Doeberitz, M.; Neumann, H. H.; Puig-Tintore, L. M.; Sideri, M.; Rehm, S.; Ridder, R.; PALMS Study Group, for the P. S. Screening for Cervical Cancer Precursors with p16/Ki-67 Dual-Stained Cytology: Results of the PALMS Study. *J. Natl. Cancer Inst.* **2013**, *105* (20), 1550–1557.

(33) Miyamoto, S.; Hasegawa, J.; Morioka, M.; Hirota, Y.; Kushima, M.; Sekizawa, A. The Association between p16 and Ki-67 Immunohistostaining and the Progression of Cervical

Intraepithelial Neoplasia Grade 2. *Int. J. Gynecol. Obstet.* **2016**.

(34) M-PER Mammalian Protein Extraction Reagent https://www.thermofisher.com/order/catalog/product/78501 (accessed May 26, 2016).

(35) Finnen, R. L.; Erickson, K. D.; Chen, X. S.; Garcea, R. L. Interactions between Papillomavirus L1 and L2 Capsid Proteins. *J. Virol.* **2003**, *77* (8), 4818–4826.

(36) Nikas, Y. J.; Liu, C. L.; Srivastava, T.; Abbott, N. L.; Blankschtein, D. Protein Partitioning in Two-Phase Aqueous Nonionic Micellar Solutions. *Macromolecules* **1992**, *25* (18), 4797–4806.

(37) Mashayekhi, F.; Meyer, A. S.; Shiigi, S. A.; Nguyen, V.; Kamei, D. T. Concentration of Mammalian Genomic DNA Using Two-Phase Aqueous Micellar Systems. *Biotechnol. Bioeng.* **2009**, *102* (6), 1613–1623.

(38) Banerjee, S.; Yalkowsky, S. H.; Valvani, C. Water Solubility and Octanol/water Partition Coefficients of Organics. Limitations of the Solubility-Partition Coefficient Correlation. *Environ. Sci. Technol.* **1980**, *14* (10), 1227–1229.

(39) Chen, X. S.; Garcea, R. L.; Goldberg, I.; Casini, G.; Harrison, S. C. Structure of Small Virus-like Particles Assembled from the L1 Protein of Human Papillomavirus 16. *Mol. Cell* **2000**, *5* (3), 557–567.